Rep. Prog. Phys. 57 (1994) 481–531. Printed in the UK

Semiconductor particle tracking detectors

G Hall

Blackett Laboratory, Imperial College, London SW7 2AZ, UK

Abstract

The last decade has seen substantial progress in the use of solid state detectors, which are now exploited on a large scale in high energy physics experiments for precise positional measurements. This article surveys the major classes of detector and the methods employed to construct them and instrument the large systems presently in use for particle tracking. Some of the most topical areas of current research and an indication of future important applications are described.

This review was received in November 1993.

0034-4885/94/050481+51$59.50

Contents

1. Introduction

Little more than a decade ago solid state detectors were hardly known in particle physics experiments. Today they provide one of the most commonly used methods of measuring charged particle trajectories in elementary particle collisions. They offer the highest spatial resolution so far achieved in large detector systems which has been their principal attraction to physicists who have been devising experiments to search for, and measure the properties of, the rare decays of short lived exotic particles. The fact that solid state detectors produce electronic signals which can be measured directly with the aid of a sensitive amplifier and processed by computer has enabled automated data collection which permits large volumes of precise measurements to be collected and analysed. High sensitivity experiments are lengthy enterprises, taking several years, but would otherwise be unthinkable.

Almost all the detectors in current use are fabricated from mono-crystalline silicon employing methods derived from the production of electronic integrated circuits. The maturity of the silicon processing industry has been a key factor underpinning the recent, rapid development of particle detectors. This technology has led to a range of detectors which have been exploited for other particle physics applications, for example as scintillation light detectors, where miniaturization of the detectors has been another attractive feature, as well as the wide spectral sensitivity. It has encouraged innovative individuals to produce novel and more complex detectors and the rapid pace of change has stimulated interest in possible further development of detectors based on other semiconducting materials and the exploitation of silicon processing techniques by more conventional detector technologies, for example using ionized gases.

Future experiments plan to exploit semiconductor detectors to create much larger systems with very small elements and high granularity. They will be used to acquire data at proton-proton and heavy ion colliders where there will be a very high density of overlapping particle tracks emerging from multiple interaction points. In the new high intensity proton machines huge numbers of particles will cross the detectors each second exposing them to radiation levels over the lifetime of the experiments comparable to those found in nuclear reactors or weapons environments. Here also, the many man years of scientific effort invested in semiconductor technology are allowing the evolution of detectors which are capable not only of survival but high performance over many years of operation.

The use of semiconductor detectors has been aided by the exploitation of microelectronics technology which has, over a similar period of time, become more accessible and permitted the construction of large readout systems of low noise amplifiers and data acquisition electronics. Some of these developments are beginning to be exploited by scientists in fields outside particle physics and it is likely that the next decade will see further utilization of position sensitive semiconductor particle detectors in other areas.

2. Background

2.1. Early history

The first semiconductor detectors were made as rectifying p-n junctions (McKay 1951),

whose properties were already well understood (Shockley 1950), using germanium because of its valence bonded crystal structure as well as the availability of suitable material. In these early measurements alpha particles were detected and the average energy to create an electron–hole pair in germanium was accurately determined to be 3.0 ± 0.4 eV. However, despite this early start with junction diodes, the earliest silicon detectors were based on surface barrier counters. The attractive features were similar to those cited today: linearity, good energy resolution and little energy loss at entrance windows, as well as compactness and fast response. In addition, for the heavy ion studies envisaged, the relative insensitivity to less ionizing particles was another useful feature (Halbert *et al* 1960). Silicon was preferred to germanium, then as now, because it could be operated at room temperature whereas germanium required substantial cooling, usually to the liquid nitrogen range, to obtain good energy resolution because of its low intrinsic resistivity and thus high dark current. By about 1960 silicon detectors could also be made in what were considered to be relatively large dimensions: up to 1 inch diameter (Dearnaley and Northrop 1964).

Although the physics of the p–n dide was quite well understood in its very earliest use as a detector, optimal methods of signal processing were not developed until some time later. This may have been related to the fact that signals from alpha particles and other nuclear fragments were generous in size, so that low noise was originally not of such great concern. However the use of semiconductor detectors for γ-ray spectroscopy applications, where high resolution was of great importance, motivated the development of matching electronics during a period when industry was rapidly developing better quality transistors. It became evident that standard techniques of signal processing did not lead to ideal noise performance and an improved understanding of the possible compromises between detector characteristics, operating conditions and amplifier design was developed. For many years, continuing to the present day, the main use of semiconductor detectors was for applications in nuclear physics and x-ray spectroscopy; much early history of the field is reviewed by Ewan (1979), Laegsgard (1979) and McKenzie (1979).

Although electronic detectors have always played an important role in particle physics experiments, for a long period from the late 1950s to the early 1970s the bubble chamber dominated the fixed target experiments which were then under way. The principal subject of investigation was the systematization of the many new particles being discovered, and the assignment of selection rules and quantum numbers which governed their hierarchy. As an experimental tool the bubble chamber provided excellent spatial resolution and complete solid angle coverage with very little intrinsic experimental bias for a wide range of reactions, whereas counter experiments were better suited to study specific reactions with small numbers of particles in the final state so that possible experimental biases could be well controlled. Using electronic detectors it was possible to acquire selected data at a high rate by triggering the data acquisition system on a characteristic signature of an interesting event, especially with the advent of position sensitive gaseous detectors (Charpak 1970) which permitted digital electronic data to be directly stored by computer and thus rapidly analysed. During this period semiconductor detectors offered little of interest to the majority of particle physicists since high energy resolution was of minor importance to this generation of experiments. A few notable exceptions pioneered the use of fully instrumented semiconductor layers in the 'active' targets of hadronic diffraction experiments for measurement of nuclear recoils (Bellini *et al* 1982a).

2.2. Charm lifetime measurements

The situation began to change in the 1970s following the discovery of the J/ψ meson which was quickly proven to be a bound quark–antiquark state in which the quarks carried a new quantum number called charm. A spectrum of mesons and baryons which contained only one charmed quark was expected and proof was soon found of their existence (Appelquist *et al* 1978). Several experimental techniques were pushed to the limit to observe decays of charmed particles which were predicted to have lifetimes in the picosecond range and accessible to direct observation provided spatial resolutions significantly below 100 μm could be achieved. Most of the successful methods (Sidwell *et al* 1983, Appel 1992) had practical drawbacks in undertaking high statistics studies of rarely produced charmed events. Bubble chambers and emulsions demonstrated sufficient spatial resolution but data taking and, particularly, analysis rates were low. Gaseous detectors were close to the limit of their intrinsic resolution. To speed progress, data samples richer in charm events were required and it was realised that semiconductor detectors might provide a means to achieve them (Amendolia *et al* 1980, Heijne *et al* 1980, England *et al* 1981).

One strategy was to improve the selection of charmed events at the trigger level. A novel feature of charmed particles is that a large fraction of them decay into three or more particles, compared to strange particles (K mesons, Λ^0, etc) which are mainly two body decays. Since charmed particles from a zero-charmed initial state, such as π or K mesons incident on an atomic target, must be produced in pairs of charm and anti-charm to conserve the quantum number, triggers that selected high multiplicity final states or recognised the increase in multiplicity signalling a decay were proposed. This was provided during analysis by measuring the signal amplitude in each layer of an 'active' target consisting of stack of instrumented silicon detectors (Amendolia *et al* 1980a). The number of particles crossing each layer could be inferred from the pulse height, assuming most of them were approximately minimum ionizing. The linearity and good intrinsic energy resolution of the detectors were key elements in this strategy.

An alternative method was to ensure that sufficient spatial resolution could be provided by detectors closest to the target of the experiment and, computing off-line, to reconstruct as rapidly as possible the trajectories of particles emerging from the collision point. Since events with no charm decay should contain only tracks which originated from the interaction point, events in which a track appeared to originate downstream of the target could contain a charm decay. Backgrounds were expected from decays of known particles, such as strange mesons and hyperons, and from secondary interactions if the target was not a single thin layer.

Making use of the excellent spatial resolution of silicon detectors has proved a more powerful experimental tool than pulse height variations in an active target. The limitations of secondary interactions, energy loss fluctuations and atomic recoils have proved to be considerable obstacles to obtaining high efficiency at the trigger level. Nevertheless, variations on the multiplicity trigger approach, by reconstructing tracks emerging from the target continue to be of interest (Adamovitch *et al* 1990, Amendolia *et al* 1990, Benso *et al* 1982, Darbo *et al* 1990), as similar challenges arise in the study of even rarer short-lived particles, such a B-mesons.

2.3. Limits to performance

The ultimate limits to the spatial precision of measurements using silicon detectors have probably been reached, although it is rare that they are a limiting factor to experiments.

They arise from diffusion of ionized electrons and holes during charge collection in signal formation and from fundamental fluctuations in the processes whereby energy is transferred from incident charged particles to the bound electrons of the semiconductor material (Landau 1944, Hall 1984, Bichsel 1988). Diffusion limits spatial measurements to a few microns in most practical circumstances. The effects due to non-normal incidence of the particle on the detector usually exceed this limit considerably (Turchetta 1993). An energetic electron ejected from an atom in the material can also significantly degrade a measurement by depositing its own kinetic energy in a region some distance from the path of the primary particle. Statistical variations in the atomic energy loss processes are quite common and, since an electron of only 10 keV energy has a range of $\sim 1\ \mu$m, fluctuations at the multi-keV level contribute noticeably to the measurement error. Most experiments find a spatial precision of 5–10 μm to be adequate, with the tails on the error distributions dominated by multiple Coulomb scattering which occurs as charged particles traverse the material contributed by the detector, electronics and unavoidable support structure.

3. Detector technology

3.1. Detector types

Using silicon as a substrate, there are two major classes of detectors: the CCD (charge coupled device), which is based on arrays of MIS (metal-insulator-silicon) capacitors and comprises a complete class of detectors in its own right, and the p–n junction diode which has become the predominant basis for constructing all other silicon detectors for particle tracking. It has virtually superseded fabrication techniques based on Schottky diode, or surface barrier, technology.

In both CCD and diode detectors a region depleted of native electrons and holes is produced in which ionization by an incident charged particle or photon generates mobile charge carriers which constitute the major part of the signal. However, at this point, the similarities cease. In the CCD the signal charge, some of which diffuses from outside the depletion zone, is trapped and stored close to the surface in a potential well whose contents are later transported to a readout node to be measured. In a diode detector the motion of the electrons and holes in the electric field within the depleted bulk material leads to a small current pulse which is amplified for measurement.

3.2. Surface barrier diodes

The earliest diode detectors were made using a very simple process in which a metal film is evaporated onto the clean surface of a semiconductor wafer. A diode is created as a consequence of the work function difference between the semiconductor and the metal and so a natural reverse bias can exist between the two materials in equilibrium. A depletion region is formed under the metal surface which can be enlarged by the application of further reverse bias voltage. The drawback of the surface barrier technique is that the diode is a rather fragile and easily damaged object. The dark current of the diode can reach levels of $\sim 100\ \text{nA cm}^{-2}$ at room temperature and can make significant contribution to noise so, in spectroscopy applications, must be reduced by cooling. However, the thin metal entrance layer offers the benefit of minimal attenuation

of the incident particle energy, which is ideal for nuclear physics experiments producing short range nuclear fragments.

For particle physics, where reaction products are usually of much higher energy, surface barrier detectors are not so attractive. Since high energy particles penetrate through typical detector thicknesses with only a minute loss of energy the ultra thin window is no special advantage. More important is the possibility of segmenting the detector into multiple elements to make more precise position measurements and limiting the leakage current so that shot noise does not obscure the small signals. A minimum ionizing particle deposits a charge of only ~4 fC in a 300 μm layer of silicon, compared to ~200 fC for a 5 MeV α particle. Although some of the earliest detectors exploited in particle physics were surface barrier devices (Bateman 1969, Amendolia *et al* 1980b, Heijne *et al* 1980, Bellini *et al* 1982a) it was soon found that p–n junction diodes offered superior performance. Planar technology for constructing p–n detectors suitable for particle physics was developed (Kemmer 1980, Kemmer 1984, Burger 1984, Hansen 1985, Holland 1989) and exploitation of the method led to the rapid development of particle physics detectors.

3.3. Junction diode principles

To explain the operation of a p–n diode it is usual to imagine the two sides of the junction originally isolated, and then brought into intimate contact. Thermal equilibrium is established as equal numbers of highly mobile electrons and holes, from the n-type and the p-type material, combine. A potential difference which prevents further current flow is maintained by the static space charge built up around the junction by the ionization of the donor and acceptor atoms in the doped semiconductor, and this region is effectively depleted of all mobile charge carriers. It is normal for one side of the junction to have been more heavily doped than the other and overall charge neutrality then implies that the depletion region extends much further into the less heavily doped side of the device; in most modern silicon detectors this is n-type.

The active detector volume is the depletion region where the electric field sets in motion mobile charges created by ionization, and generates a signal current pulse. The size of the depletion region can be increased up to the point where the complete thickness of the semiconductor wafer is depleted by applying further reverse bias voltage. More detailed accounts can be found in Damerell (1986), Klanner (1988) and Peisert (1992). Due to the abence of mobile charge carriers, there is almost no current flow except when ionization generates electrons in the conduction band. The small leakage currents originate mainly in thermal excitation of electrons into the conduction band, mostly via energy levels within the forbidden energy gap caused by impurities either in the raw material or introduced during processing, or from short-lived states at the surface of the material.

Noise in the system is not optimized by minimizing leakage currents alone, since the other important parameter of a diode detector is capacitance. High frequency components of the current signal can be partially shorted to ground by the detector capacitance whereas the spectrum of thermal noise in the amplifier is not attenuated in the same way. The input capacitance also has a multiplicative effect on the amplifier noise. Thus a large detector capacitance degrades the achievable signal to noise ratio. Depending on time constants used in the amplifying system, electronic noise is mainly determined by leakage currents or device capacitance.

Elementary detectors based on junction diode technology are widely used in particle physics (Ansari *et al* 1989). Position measurements with a precision of a few mm or less are valuable in localizing high energy electromagnetic showers in calorimetric detectors. This is a relatively simple task for a silicon detector with coarse strips and the linearity and lack of gain are advantageous in ensuring accurate measurements over long periods. The detectors can be made in shapes which fit readily into awkward locations with minimal inactive areas, such as the forward regions of colliding beam experiments (Fernandez *et al* 1990). Photodiodes are convenient detectors for scintillation light produced in electromagnetic calorimeters, and are manufactured like other silicon detectors except for omission of the metal contact over most of the diode surface. They have high quantum efficiency over a wide spectral range and are compact, robust and can be used in high magnetic fields. Operated with thin depletion layers, fast charge collection and sufficiently low capacitance for adequate electronic noise have been demonstrated. Large scale use of silicon photodiodes for readout of bismuth germanate crystals by the L3 experiment (Ferroni *et al* 1991) and of caesium iodide by the CLEO experiment (Bebek 1987) have proven the technique, although details are beyond the scope of this article.

3.4. Modern detector fabrication

The essential precursor of the modern planar process (figure 3.1) for silicon particle detector manufacture is oxidation of a clean silicon wafer. Bare silicon rapidly oxidizes if exposed to air but only a fragile, few Å thick layer is produced. It offers little protection from contaminant atoms which can diffuse into the silicon during high

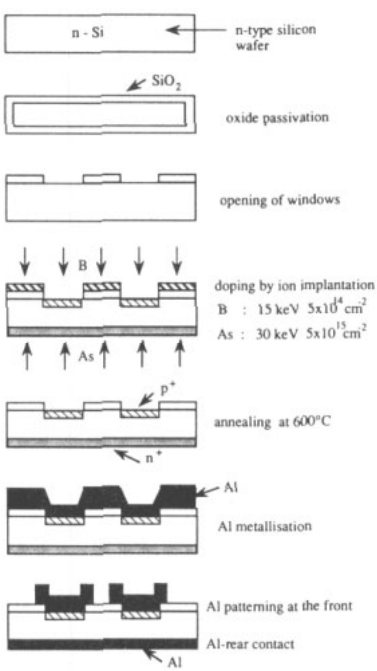

Figure 3.1. The major steps in the planar fabrication process of silicon strip detectors (after Kemmer 1980).

temperature processing stages. In contrast, a thermal oxide a fraction of a micron thick is an optically transparent barrier with excellent dielectric properties. If grown under the right conditions, it has desirable passivation properties by completing covalent bonds at the silicon surface where silicon atoms cannot share electrons with symmetrically positioned neighbours. This is very important electrically in controlling the density of surface states which contribute to surface currents and breakdown phenomena. The oxide also conveniently provides a layer on which the photolithographic mask steps used in microelectronic manufacture can be carried out, which means that fine features can be implanted into the silicon to create the doped areas necessary for diode fabrication.

The main steps in the processes now in use for diode detector and electronic circuit fabrication are quite similar (Sze 1988), although detector manufacturers optimize their own procedures to ensure reliable and robust production, usually with process variations treated as commercially sensitive information. Wafers are chemically and mechanically polished to a high standard before processing begins, since subsequent steps are influenced strongly by surface quality (Ravi 1981). Surface imperfections act as nuclei for crystal defects produced during oxidation and the formation of micro-cracks at the edge of the wafer can lead to breakages during handling. Stringent cleaning of the wafers is also vital before they are oxidized at a temperature of, typically, 950–1100 °C for several hours in dry oxygen or steam where the high temperatures are necessary to ensure reasonable oxidation times. Wet oxidation, using steam, is required for the thick oxides of $\sim 1\ \mu$m usually produced.

During these stages a small percentage of hydrogen chloride or other chlorinated chemical is incorporated in the furnace environment to improve the oxide quality by the gettering action of the chlorine. Some of the undesirable metallic contaminants form volatile chlorine species at high temperatures and can thereby be removed, preventing them from diffusing into the silicon substrate. Other gettering processes, which make use of the presence of phosphorus, polysilicon or surface abrasion prior to oxidation (Sze 1988, Holland 1989), are also employed. They work by deactivating potentially damaging contaminants by trapping them, either in a chemical form, e.g. using phosphorus, or mechanically, using the damage sites in the crystal which are later etched away.

Photolithographic methods are then used to etch windows into the oxide for subsequent ion implantation or diffusion steps. A layer of photoresist, a photosensitive polymer, is spun onto the wafer in liquid form to ensure an even thickness. It is hardened by baking and exposed to ultraviolet light through an opaque chrome pattern on a glass mask plate, which damages the polymer chains so that the exposed regions can be dissolved in a developer. The oxide surface beneath is then etched away using buffered hydrofluoric acid, opening windows to the silicon surface. Wet etching, employing liquid agents, is widely used for detector manufacture. Although dry etching techniques, using highly reactive radicals created by RF plasmas or ion beams, are frequently employed to etch silicon nitride and polycrystalline layers because of the improved control of circuit dimensions they permit, they have the drawback of less selectivity between materials. In contrast to electronic circuit manufacture, the dimensional tolerances for silicon detectors are modest, with feature sizes usually greater than $5\ \mu$m. However, the large device dimensions, with detectors occupying most of the wafer area, restrict the possibility of local alignment and focusing employed for integrated circuit manufacture. Similar constraints apply to the optical masks, requiring most masks for microstrip detectors to be made using electron beam lithography to achieve the necessary specifications.

The diode junctions are formed by implanting or diffusing doping atoms into the silicon surface exposed in the earlier etching stage. The implantation energy must be a compromise between penetration of the oxide by the ions, and thus doping of undesired areas, and the depth of the junction required; typical energies for boron implantation are 10–100 keV. Annealing of the wafer is then carried out to activate the implanted ions by allowing them to take up normal lattice sites and repair the surface damage caused by ion impacts. Where diffused junctions are created a layer of thermal oxide is grown in a boron rich environment; the boron atoms then diffuse into the silicon during an annealing step carried out at temperatures around 600–800 °C. In very shallow junctions high electric fields can be present at extremities which can contribute to low breakdown voltages and guard ring structures can play an important role. Although modelling of the junction region is possible by numerical semiconductor simulation, designs have mainly been optimized by empirical methods.

Implantation or diffusion of arsenic or phosphorus into the back surface of the wafer creates a highly doped n-type region which ensures a good ohmic contact between the metallization subsequently applied and the silicon beneath. Aluminization of the surfaces then follows, with final photolithographic steps to pattern the metal for the individual diode contacts.

As described, the overall process is relatively simple and comprised of a small number of important stages. However each of these steps contains many sub-processes, many of which are vital to the final performance of the completed device, and significant variations between manufacturers are also common. The basic process has also been supplemented by additional steps to create further metal, polysilicon or silicon nitride layers which permit coupling capacitors, bias resistors and complex contacts to be incorporated into the detector. Thus, although detector fabrication is still less complex than modern electronic processing, the technology is similar and in some details more stringent.

3.5. Detector operation

The major differences between the fabrication of detectors and microelectronic circuits arise from the raw material. Silicon of high resistivity is essential for detector production because there is a practical limit to the operating voltage which can be applied to a silicon detector before breakdown occurs and the depth of the depleted region of a p-n diode is inversely proportional to the doping concentration. To deplete an n-type layer of thickness d, with donor concentration N_D, a voltage V_D is required, where

$$V_D \approx qN_D d^2/2\varepsilon \approx 7.6 \times 10^{-10}\,[V\,\mathrm{mm}^{-2}]\,N_D d^2$$

where q is the electronic charge and ε is the dielectric constant of silicon. For practical operating voltages, doping concentrations of 10^{11}–10^{12} cm^{-3} are required, corresponding to resistivities of a few kΩ cm. In comparison silicon for electronic circuits has a typical resistivity in the range 0.1–10 Ω cm.

Low dark currents in operational detectors are of great importance because of their contribution to electronic noise and in practice bulk leakage currents of $\sim$1 nA cm^{-2} can be achieved. To reach this level scrupulous attention must be paid to processing conditions and handling of the wafers and although high standards are routine in large scale electronic manufacture, the small scale, custom nature of detector production creates extra problems for the detector manufacturer. Because leakage currents arise from electron and hole transitions across the bandgap they are particularly sensitive to

energy levels in the mid-gap region. In the bulk of the silicon the atomic species which cause these states are well known (Sze 1981) and can be controlled while at the surface the crystal orientation, oxidation conditions, high temperature process steps and annealing stages are sensitive parameters. Minor modifications to the fabrication process to optimize detectors for a specific purpose or develop new aspects of the technology can have major repercussions for quality, at least temporarily.

Detector sizes are largely determined by the dimensions of high resistivity silicon wafers. Three and four inch diameter wafers are commercial standards, with larger sizes now favoured by most manufacturers; five inch diameter wafers are being introduced. By normal microelectronic standards, a device covering a large area of the wafer would be a non-commercial proposition since the yield, or fraction of devices meeting acceptable specifications, would be expected to be very small. This can only be overcome because diode detectors are relatively simple in comparison to electronic circuits and every wafer experiences quality control in most steps of the manufacturing process. Thin wafers are generally used as, for tracking detectors, there is normally a requirement to limit material to minimize secondary interactions, photon conversions and multiple Coulomb scattering of charged particles. 300 μm is a convenient compromise between signals of sufficient size for good signal to noise ratios and ensuring the high yield required to limit cost. The raw material, although expensive compared to standard electronic grade silicon (von Ammon and Herzer 1984), is not a major part of the cost of detectors. The number of processing steps and the probability of breakages when using thin substrates are the two main factors limiting the yield.

3.6. Microstrip detectors

The most widely used semiconductor device for particle tracking is the silicon microstrip detector (figure 3.2). In its simplest form this is constructed as an array of diodes on a single silicon wafer. Typical dimensions are 8–15 μm wide diodes on 25–50 μm pitch. The maximum length of 5–8 cm is determined by the size of high resistivity silicon wafers; longer detectors are constructed by bonding together shorter units. To operate diodes as detectors, either a low input resistance amplifier or a capacitively coupled amplifier with a large bias resistor is required, so that the signal path appears as a small

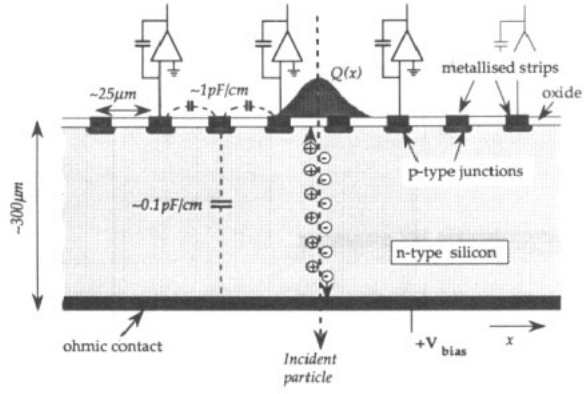

Figure 3.2. Schematic cross section through a silicon microstrip detector. Diffusion distributes the collected charge over multiple strips and capacitive charge division between the readout amplifiers allows position interpolation.

impedance to ground. The DC coupled system is more difficult to implement with, now widely used, CMOS readout technology and AC coupling is often preferred to isolate leakage currents from the amplifiers since high levels can lead to a loss of dynamic range in the readout system or necessitate special amplifier design. Discrete capacitors and resistors are bulky components and several methods have been developed to match them to the VLSI electronics now in use by integrating them into the detector structure.

Detectors with biasing via a narrow p^+–n–p^+ junction between the strips and a common bias line have been built (Kemmer and Lutz 1987, Batignani *et al* 1991) in which a reach-through diode structure (figure 3.3), similar to that developed for microwave applications (Chu 1972, Lohstroh *et al* 1981), is produced to hold the strips a few volts from the bias line. Depletion zones exist around each p-type region and, as the bias voltage is increased, they eventually make contact. As further bias is applied, the unconnected (microstrip) junction is slightly forward biased with respect to the nearby substrate and a charging current of holes flows until the potential barrier is restored. In the absence of leakage currents, equilibrium between the p-type strips and the bias line is reached with a small potential difference between them. Leakage currents from the strip modify this only slightly. Greater control of the voltage offset between bias line and strip can be achieved by adding a metal gate over the oxide above the n-type region so that a field-oxide MOS transistor (FOXFET) is produced (figure 3.3d) and allows additional flexibility in the detector design (Allport *et al* 1991).

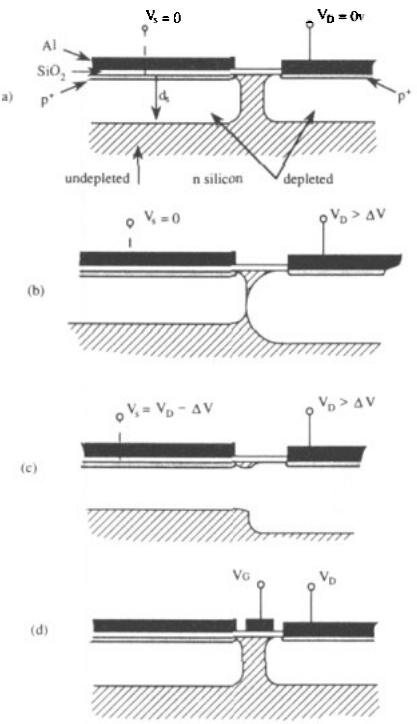

Figure 3.3. Biasing of microstrips through a p^+np^+ structure by the reach through effect (*a*)–(*c*). The depletion volume is extended from the bias line by the applied voltage until adjacent p-type regions are in contact, in which the back to back diodes ensure a high resistance. The addition of a metal gate (*d*) between the p-type strips allows additional control (FOXFET).

Polysilicon layers are commonly used for producing resistors and connecting lines in MOS electronic technology; using this method and controlling the sheet resistance by ion implantation high value resistors have been produced by several manufacturers with values up to 10–20 MΩ (Caccia *et al* 1987). The use of polysilicon adds additional steps to the manufacturing process and the resistors take up a little more space than reach-through structures but are reliable, uniform and radiation hard (Edwards *et al* 1991, Pitzl *et al* 1991).

Arrays of external oxide coupling capacitors on quartz substrates have been used (Batignani *et al* 1991) to minimize modifications to the detector manufacturing process although they add more material to the system and can have limited breakdown voltages. The coupling capacitor should ideally have a value considerably larger than that of the detector element, yet achieve this in a small space. They can be realised in a standard MOS technique, by growing a thermal oxide on top of the diode prior to subsequent metallization (Caccia *et al* 1987), which has also been used with FOXFET biased detectors (Allport *et al* 1991). The value of the capacitor is determined by geometry; for realistic values of a 10 μm wide strip and an oxide thickness of 0.2 μm a coupling capacitor of 17 pF cm^{-1} can be produced, which is still significantly larger than the typical strip capacitance of 1–2 pF cm^{-1} (Sadrozinski *et al* 1993, Hall *et al* 1993, Yamamoto *et al* 1993, Holmes-Siedle *et al* 1993b). The main weakness of this method is the possibility of 'pinholes' in the oxide which lead to a fraction of defective strips with low voltage breakdown between metal and diode. This is a virtually unavoidable problem caused by topological deformation of the surface and local thinning of the oxide.

For both internal and external oxide capacitors the operational voltage is limited by the breakdown field of 10^7 V cm^{-1} of silicon dioxide. In practice, operational conditions are usually chosen to limit voltages across the oxide to values less than 100–150 V. By adding an additional dielectric layer the probability of pinholes can be reduced to negligible levels and the use of a 0.1 μm silicon nitride layer has been demonstrated to be extremely effective in guaranteeing high voltage operation (Holmes-Siedle *et al* 1993b, Bosisio 1993), although again adding to the complexity of the fabrication process.

3.6.1. Double sided microstrips. In most experiments there is a desire to measure both spatial coordinates in the plane of the detector, usually with minimum additional material. It was therefore logical to obtain both coordinates from a single detector, despite the substantial increased complexity of manufacturing detectors to achieve this. A current pulse in the detector can only be sensed once from each surface without loss of amplitude, and reduction of signal to noise ratio, so double sided readout detectors were devised to solve this problem, although there have been suggestions for novel designs which would limit the processing to only the diode surface (Huhtinen *et al* 1993) at the expense of loss of signal and extra inter-element capacitance.

There are two principal problems of double sided detectors: fabrication of elements on both wafer surfaces and the electrical behaviour of the second surface. The development is specific to particle physics applications, since commercial electronic technologies rarely process both sides of a wafer, and the extra handling requires special precautions and equipment to ensure that quality is not degraded. However a more fundamental problem is that of forming individual elements on a surface whose usual purpose is to act only as an ohmic contact. Strips formed by highly doped regions on an n-type sustrate create only n^+–n contacts and not diodes so poor interstrip isolation is expected. The problem is enhanced by the fact that the oxide which separates the n^+ strips

contains a high density of fixed, positive charge which induces a sheet of negative charge just beneath the silicon-oxide interface. This electron accumulation layer effectively connects n^+ strips together (figure 3.4(*a*)) and it is essential that between strips this should be broken so that signals are not distributed over many elements. Two methods have been devised: the implantation of p^+ field stops and the construction of MOS field plates (figure 3.4).

In the p-stop method (Batignani *et al* 1988, Holl *et al* 1989, Yamamoto *et al* 1993), each n^+ strip issurrounded by a highly doped p^+ region, which is not biased. Once the detector is depleted the p-stops charge to a potential required by the p^+–n–p^+ reach-through structure formed across the wafer. The magnitude of the potential difference between the n^+ strip and the p-stops depends on the geometrical layout of the strips and on the doping of the p^+ region but they isolate each n^+ strip from its neighbour with very large interstrip resistance. Bias resistors have been constructed by narrow electron accumulation channels confined by the p-stops, which connect the bias contact to each strip.

The alternative field plate method has been used for detectors where coupling capacitors are integrated onto the strips since it can be implemented with no extra processing steps (Avset *et al* 1990, Brenner *et al* 1992, Brenner *et al* 1993a). The metallization over each strip is extended sideways over the oxide beyond the implanted region beneath it. In the MOS gate-like structure formed the accumulation layer beneath the oxide can be broken if the polarity of the metallization is negative with respect to the substrate. This is conveniently arranged by biasing the detectors with a positive voltage at the n^+

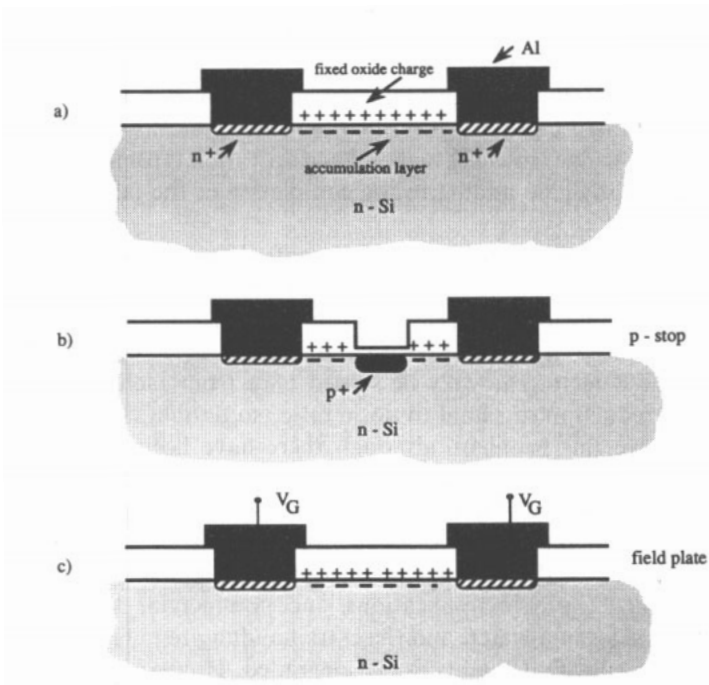

Figure 3.4. Microstrips on the ohmic detector surface are linked by the electron accumulation layer induced at the oxide interface (*a*) without special precautions. Two methods used to overcome this are the implantation of p-stops (*b*) or the use of an MOS gate structure (*c*).

junctions and allowing external electronics, which are close to ground potential, to bias the metallization.

Both ac coupled and dc coupled detectors are metallized along their entire length so there is an electrical contact to each diode, which is then connected to a readout amplifier. The connections are made by ultrasonically bonding aluminium wire between the detector and amplifier or printed circuit board. The high density of connections has been one factor necessitating the development of microelectronic amplifiers so that minimum external capacitance is added to the detector and the readout circuits are matched to the detector elements. However, it is extremely difficult to make bonds at less than 50 μm pitch. This is significantly denser than normal industrial standards, so finer strips must be fanned out by metallization on the surface of the silicon, which has the danger of parasitic MOS structures as well as extra capacitance.

3.7. Silicon drift chambers

The microstrip detector can be viewed as the solid state analogue of the gaseous multiwire proportional chamber; the solid state analogue of the gas filled drift chamber is the silicon drift chamber (Gatti and Rehak 1984).

The basis of the silicon drift chamber is a wafer of high resistivity n-type material with p-type junctions implanted into both surfaces. It can be imagined as two p-n diodes back to back, and with no applied voltages a region of the substrate underneath the junctions is already depleted. The undepleted conducting layer is confined to the centre of the wafer and can be electrically connected to an ohmic contact, for example at the surface of the wafer outside the p-type implant. If reverse bias is applied to the junctions by grounding the n-type conductor and applying identical negative voltages to the p-type junctions the depletion zones on both sides of the wafer extend into the bulk, and with sufficient bias eventually make contact.

The fully depleted detector has a potential distribution with a minimum for electrons at the centre of the wafer. The electric field transports charge generated by ionization across the wafer, electrons to the centre and holes towards the surface. If an electric field parallel to the wafer surface is also provided electrons can drift within the bulk. Computations of the potential distribution by solution of Poisson's equation show the characteristic parabolic form which confines and transports the electrons (figure 3.5).

The first working detectors were constructed as p^+-n-p^+ diodes with the p-type implants fabricated as a series of identical strips on both surfaces (Gatti *et al* 1984). The drift field was provided by externally biasing opposite strips to the same voltage but grading the potential so that strips furthest from the anode were at the highest (negative) potential relative to ground. Later detectors (Rehak *et al* 1985, 1986) incorporated guard strips, anodes and implanted potential dividers to bias the strips and modify potential distributions to ensure ideal charge collection characteristics.

The electron cloud arrives at the collecting anode after a delay with respect to the original ionizing event and one coordinate of the interaction can be measured using its arrival time. A second coordinate can be obtained by segmenting the anode. Drift fields of ~30–1000 V cm^{-1} have been used, leading to drift velocities of ~0.5–15 μm ns^{-1} at room temperature. If the interaction time is well defined by an external trigger this can permit a very precise measurement which makes possible large reductions in the number of readout channels at the expense of more complex electronics. The limiting factors come from variations in resistivity from the raw material (Avset *et al* 1991, Vacchi *et*

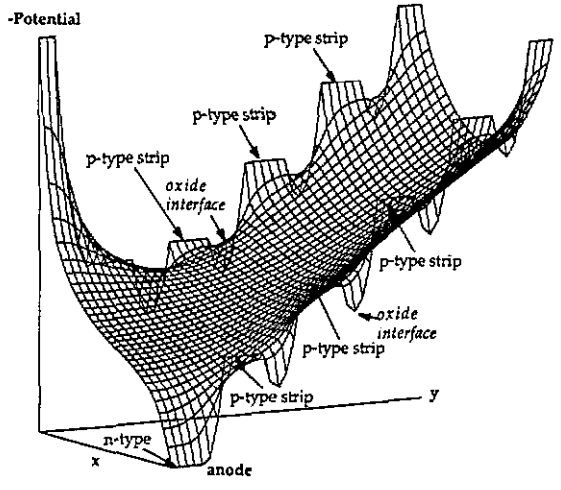

Figure 3.5. A simulation of the potential distribution in a silicon drift detector. Equal negative voltages are applied to opposite p^+ electrodes to deplete the detector and create a minimum for electrons, giving rise to the characteristic gutter-like potential. In the anode region the potentials are chosen to ensure migration of the electron cloud towards the n^+ anode.

al 1993) and the control of the detector environment since electron mobility in silicon is sensitive to temperature changes, as $\sim T^{-2.4}$.

Another advantageous feature of the silicon drift chamber is very low capacitance which, because of its implications for noise, can lead to remarkable improvements in energy resolution. It is determined by the geometrical capacitance of the anode and is practically independent of detector area. Detectors have been constructed with capacitance of 0.1 pF for a detecting area of ~ 1 cm^2 and room temperature leakage current of 1 nA; further improvements are achieved by cooling (Rehak *et al* 1989). At such small values of detector capacitance it is important to match the detector capacitance to the input transistor for optimum noise, as well as reduce stray capacitances to an absolute minimum.

To date, most of the results from silicon drift chambers have come from prototype studies although a few have been used in experiments (Chen *et al* 1992, Vacchi *et al* 1993). Because of the fact that they require processing on both wafer surfaces they are considerably harder to produce than standard microstrip detectors and the readout of the whole area from a small number of anodes means that detector quality, in particular leakage current, is of crucial importance. Large potential differences, of up to several kV, are required to operate wafer size detectors. These factors have so far discouraged significant commercial interest in production of drift detectors.

3.8. Charge coupled devices

The CCD is a detector based on an area of MIS capacitors, actually employing a polysilicon, rather than metal, gate structure on the surface (Figure 3.6(a)). By applying sufficient positive gate voltage it is possible to deplete under the oxide surface and the potential well created within the silicon under the oxide can store electrons produced by ionization. Adjacent polysilicon electrodes on the silicon surface biased to different voltages confine the charge under the polysilicon gate. Potential barriers formed by

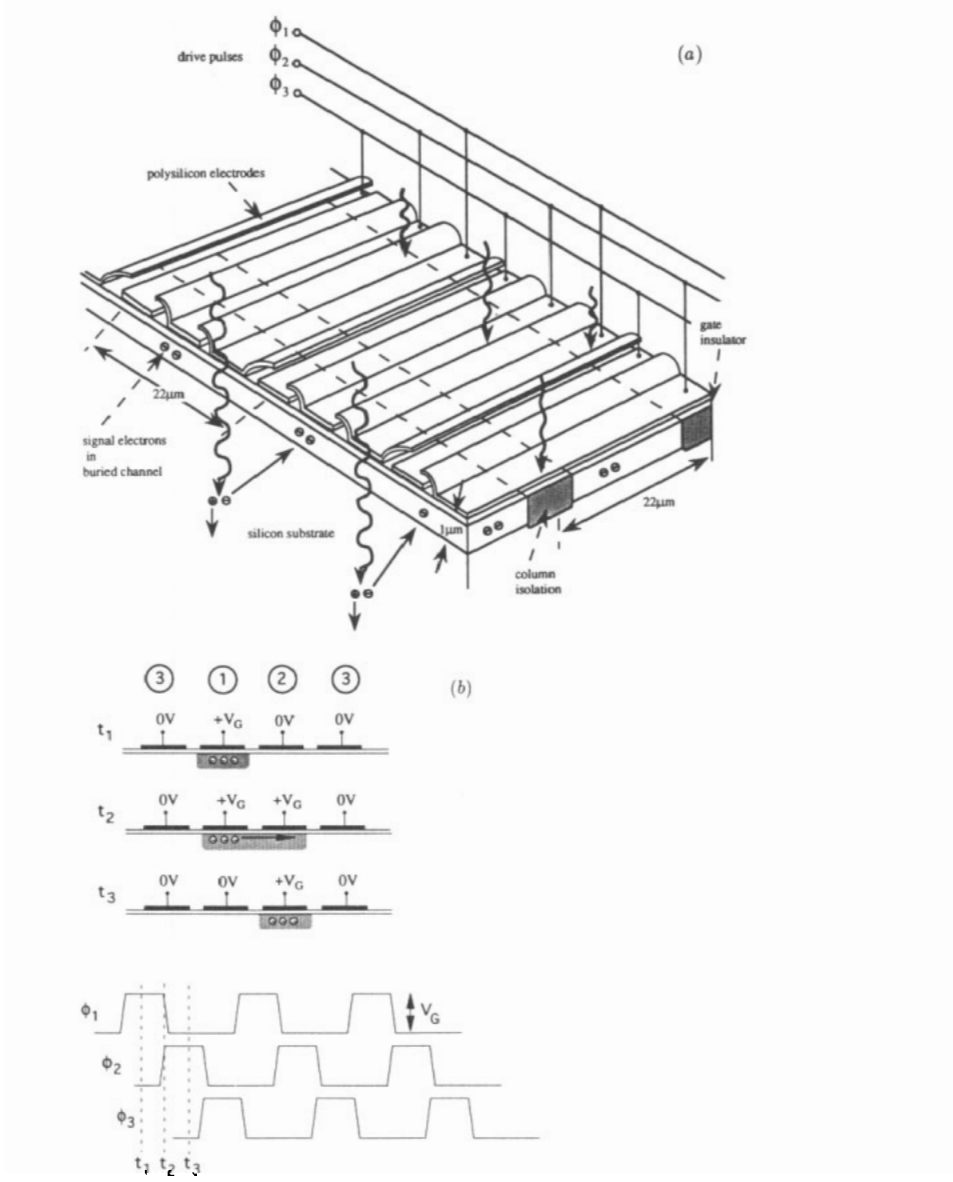

Figure 3.6. The structure and operation of a CCD (Wells and Pounds 1993). (*a*) Charge generated by ionization is confined within a pixel by potential barriers created by voltages ϕ_1 and ϕ_3. Positively biasing the intermediate electrode to ϕ_2 collects the charge. (*b*) The sequence of clock pulses used to shift the charge in a CCD from pixel to pixel.

p-type channel stops in the orthogonal direction define a pixel. Charge is transported through the array by sequentially varying the voltages on adjacent electrodes and forcing the charge to flow from one potential well to its neighbour (figure 3.6(b)). The signals are moved simultaneously by row along the columns of the CCD to a one-dimensional readout register where they are clocked individually to the readout node and sensed by a single transistor buffer amplifier.

The simplest (surface channel) type of CCD has been used in commercial video devices but it is unsuitable for charged particle and x-ray detection because of the relatively low charge transfer efficiency (CTE) due to charge trapping at the surface. This comes about because of the close proximity of the potential minimum to the oxide interface where a high trap density is present. Inefficiencies of less than one part in 10^5 are required because of the large number of transfers to the readout node.

A more effective structure which is used for all scientific applications is the buried channel CCD which is manufactured by creating higher resistivity n and p doped epitaxial layers on the surface of a low resistivity p-type silicon wafer (Damerell 1986). The structure can be biased from the gate and a substrate connection to form a potential minimum for electrons a short distance ($\sim$1 μm) from the oxide interface, improving the CTE considerably. The overall active thickness is about 20 μm, of which about 7 μm is depleted, although deeper depletion CCDs are now available (Wells and Pounds 1993).

Charged particles generate ionization both in the depletion region and undepleted remainder of the epitaxial layer. The potential barrier formed at the p-p^+ interface prevents escape of charge from the epitaxial region to the substrate (Damerell *et al* 1989). Charge is collected quickly from the depleted region but diffuses more slowly from the undepleted volume and is eventually shared between several pixels. This is an advantage for position measurement as the centroid of the charge cluster can be located and used to improve the spatial resolution. Pixel sizes of 20–30 μm are used in CCDs of up to 4000 × 4000 elements in size, although such large devices have not yet been used for particle detection; more typical are CCDs of 9 mm × 13 mm. Resolutions of 4.3 μm have been achieved (Bailey *et al* 1983) and 5–8 μm has been attained in a large scale application (Agnew *et al* 1993).

For scientific applications signals are generally small, corresponding to the detection of a few keV x-ray in astronomical applications or the deposition of 1000–2000 electrons from a MIP crossing the thin sensitive layer (Bailey *et al* 1983). However, despite the small signals, a special advantage of very thin detectors is the relative rarity of knock on electrons which can significantly distort the position measurement in thicker detectors. The entire dark current from the CCD is collected, like the signal, at the readout node so the detector is cooled, usually to around −100 °C, to limit shot noise. Readout speeds are limited by the need to minimize the noise. Astronomical applications require noise levels of a few electrons and readout times in the ms range are used while in particle physics some parts of the readout can be run at speeds of up to 10 MHz and still achieve excellent signal to noise performance.

3.9. Other semiconductor materials

For particle physics applications, silicon has proved to be quite adequate to date, although there are some doubts about the performance of future detectors in high radiation environments. For this reason there has been some interest in alternative materials, which include gallium arsenide and diamond. For applications such as x-ray detection, semiconductors with higher atomic number than silicon are of interest (Cuzin 1987); the most advanced are germanium and gallium arsenide. Amorphous silicon has been proposed as a means of instrumenting large areas at low cost with integrated electronics. A comparison of the properties of some relevant materials is given in table 1.

3.9.1. Germanium. Because of its high atomic number and the fact that it requires detectors to be operated cryogenically, with consequent additional material, germanium

Table 1. (Selberherr 1984, Hikasa *et al* 1992, Franklin *et al* 1992, Landolt-Börnstein 1985, Beaumont *et al* 1993, Sze 1981, Ma and Dressendorfer 1988.

Property	Silicon		Germanium	Gallium Arsenide	Diamond	SiO_2
	Crystal	Amorphous				
Z	14		32	31/33	6	
A	28.1		72.6	144.6	12.0	44.1
Band gap (eV)	1.12	~1.9	0.66	1.42	5.5	9
Energy to create e-h pair (eV)	3.55	~5	2.85	4.1	~13	17
Density ($g\,cm^{-3}$)	2.33		5.33	5.32	3.5	2.2
Dielectric constant ($pF\,cm^{-1}$)	1.05		1.42	1.16	0.50	0.35
Radiation length ($g\,cm^{-2}$)	21.82		12.25	12.2	42.70	27.05
Average minimum ionizing energy loss† ($MeV\,g^{-1}\,cm^2$)	1.66		1.40	1.45	1.78	1.72
Average signal‡ (electrons/μm)	110	~80	260	173	~50	20
Electron mobility§ ($cm^2\,V^{-1}\,s^{-1}$)	1450	~1	3900	8500	1800 (crystal)	~20
Hole mobility§ ($cm^2\,V^{-1}\,s^{-1}$)	450	~0.05	1900	400	1200 (crystal)	10^{-4}–10^{-6}
Intrinsic electron density(n_i) (cm^{-3})	1.45×10^{10}		2.4×10^{13}	1.79×10^{6}		
Intrinsic resistivity (Ωcm)	2.3×10^{5}	10^{9}–10^{11}	47	10^{8}	$>10^{11}$	

† Most probable energy loss in thin layers is less, and does not scale linearly with thickness.
‡ Observed signals depend on charge collection efficiency. Only in germanium and silicon is this close to 100%.
§ Typical values. For more precision, consult original sources.

has not been so widely used as silicon for tracking applications in particle physics. It is more commonly employed for spectroscopic studies where these features can be used to advantage. However germanium detectors have been exploited on a number of occasions, most notably in the series of active target experiments carried out in several laboratories by Italian collaborations. In the CERN NA1 experiment 5 mm thick layers were segmented into strips of 50 μm or 100 μm pitch to build a target of volume 5 mm × 5 mm × 20 mm (Amendolia *et al* 1984) using the beam incident parallel to the strip surface. They were operated at ~100 K with a depletion voltage of 450 V. At Fermilab, for the E687 experiment, a 5 mm × 5 mm × 20 mm monolithic germanium detector, with an electrode on the bottom and 40 100 μm pitch strips implanted onto the top surface orthogonal to the incident beam direction, was constructed to improve the sensitivity to shorter lifetimes (Bellini *et al* 1984). The same thickness of germanium produces larger average pulse heights than silicon, so greater effective granularity can be achieved by using more layers if increased backgrounds can be overcome.

An interesting application of germanium for production of semiconductor drift chambers took advantage of the fact that high purity crystals often exhibit an increasing n-type impurity concentration towards the tail of the ingot due to phosphorus segregation during crystal growth (Luke *et al* 1985). The concentration gradient in the germanium was used to create a built-in drift field in drift chambers 3 cm × 3 cm × 300 μm in

size. With drift distances up to 27 mm a spatial resolution of below 500 μm was achieved over the active area of ~25 mm × 25 mm.

3.9.2. Gallium arsenide. The attractions of gallium arsenide as a particle detector include its potential radiation hardness, high electron mobility and compatibility with opto-electronic devices constructed on the same substrate. Up to now these features have not been fully realised because of the quality of commercial GaAs, for which a wide range of methods are used to produce wafers for electronic device fabrication (Landolt-Börnstein 1985). Whether this will change probably depends largely on other commercial demands. However substantial improvements in raw material have been realised in recent years, leading to some hopes that useful detectors could soon be produced on a significant scale.

GaAs is a direct band gap semiconductor with short intrinsic carrier lifetimes: around 5 ns at room temperature. Longer lifetimes are obtained in an electric field but the presence of traps has the opposite effect and high fields have been found necessary to ensure good charge collection properties, hence the ability of detectors to sustain high fields without avalanche breakdown is important. The specific energy loss of gallium arsenide should require thinner layers than silicon to observe similar size signals from minimum ionizing particles, although this represents significantly more material because of the shorter radiation length. However, in practice many detectors do not exhibit full charge collection efficiency which makes the comparison even less favourable.

GaAs ionization detectors have been fabricated using various epitaxial techniques (liquid phase, vapour phase and molecular beam). They produce high purity single crystal material with free carrier concentrations of $\sim 10^{14}$ cm^{-3} and active depths limited typically to less than 100 μm. Excellent charge collection efficiencies have been observed (Sumner *et al* 1993) but the detectors are limited in size and by the expense of the technology. Thicker detectors are possible using liquid encapsulated Czochralski (LEC) semi-insulating GaAs which contains dopants (e.g. Cr) added to increase material resistivity through creation of trap centres (Spooner *et al* 1991). This has been widely used to produce detectors on larger size wafers employing several fabrication techniques, including Schottky barriers and p-i-n structures (Beaumont *et al* 1992, McGregor *et al* 1992, Chmill *et al* 1993).

The depletion mechanism is somewhat more complicated than in silicon and depends on details of the raw material (McGregor *et al* 1992, Beaumont *et al* 1993). In undoped semi-insulating LEC material, there is an excess of deep donors over shallow acceptor impurities and semi-insulation is achieved by compensation between shallow and deep levels. The electrical properties are controlled by the intrinsic compensation mechanism and the high density of traps, impurities and lattice defects. A non-uniform space charge density arises from ionized shallow donors and acceptors, ionized deep levels and electrons in the conduction band, in a similar manner to poor quality crystalline silicon (Dabrowski and Korbel 1989). The local space charge density under bias depends on the energy of traps relative to the Fermi level. In a detector, the field distribution and charge collection are therefore hard to predict, in addition to trapping effects. Studies have demonstrated significant differences in performance between detectors constructed on different starting material (Beaumont *et al* 1992) and variations are also observed which depend on bias and substrate thickness as well as the fabrication technology. The best LEC detectors have shown charge collection efficiencies of 80%

for layers up to 300 μm thick (Beaumont *et al* 1993), although ~50% is at present more typical, but thicker layers have reduced efficiency.

Experience to date with gallium arsenide demonstrates the advantages of working with a widely used commercial semiconductor, like silicon, where the vast effort by industry to develop materials and technologies can be exploited by detector builders. Much work is still required to characterize and understand the different raw materials and it is likely to be still some years before GaAs detectors will find significant use.

3.9.3. Amorphous silicon. Hydrogenated amorphous silicon is a form of silicon where most Si-Si bonds are slightly distorted from their crystalline value, leading to medium and long range disorder. Compared to the crystalline state, the amorphous state is not well defined and there is a continuous transition from amorphous to microcrystalline material. However, disorder does not prevent the formation of conduction and valence bands but it does lead to some blurring of the band edges and an extension of the density of states into the forbidden band. Unsaturated, or dangling, bonds appear as states near the middle of the band gap. Hydrogenation is required to saturate defects and reduce the density of gap states to obtain semiconductor properties; the relatively large amounts (up to ~50 at%) justify treating the material as a binary alloy (a-Si:H).

The disorder in the material, and the presence of traps, leads to low carrier mobilities (Street 1983, Equer and Karar 1989) because the large density of shallow states leads to a high probability of trapping and thermal detrapping. High electric fields are required to overcome the low mobilities. Depletion layer formation occurs in a different way than crystalline silicon as it is controlled by deep states, which can be positive, negative or neutral.

The attraction of the material is the possibility of large area fabrication in a low cost process, in contrast to crystalline technology which requires high quality materials and leads to devices with high cost per unit area whose size is limited by ingot diameter. Large surface area amorphous silicon devices are being developed commercially for purposes such as computer displays and scanning devices, where pixels are individually instrumented with thin film transistors. Applications such as x-ray detection would benefit considerably if fully instrumented devices ~30 cm × 30 cm with no significant dead areas could be constructed. This still seems to be some years away.

Amorphous silicon detectors usually exhibit a sandwich structure consisting of a thin (10–100 nm) p and n doped layer surrounding a thicker (5–50 μm) layer of material which is not intentionally doped. p–i–n diodes are typically fabricated by depositing layers of amorphous silicon on a glass substrate covered with a conducting metal electrode. A further metal electrode is then deposited by evaporation or screen printing and devices are stacked together in series to increase the available thickness and reduce the overall capacitance. Ionizing signals have been detected, from alphas and low energy protons (Perez-Mendez *et al* 1986, Equer and Karar 1988), although with poor signal to noise because of the large capacitance, and large fields are required to reach charge collection saturation. The details of the charge collection process are still obscure; several mechanisms probably contribute to the slow and incomplete collection (Equer and Karar 1988).

Due to their small thickness, present detectors are not sufficiently sensitive to permit detection of individual minimum ionizing particles. However, direct detection of β electrons has been achieved using a 5 μm thick Schottky barrier amorphous silicon detector (Kaplan *et al* 1988) by triggering on an external signal and averaging several hundred pulses to reduce electronic noise. A peak was observed whose centroid is

shifted compared to a randomly triggered spectrum which corresponded to a signal of ~160 electrons and a signal to noise ratio ~1.

Minimum ionizing particle detection in amorphous silicon might be feasible with small pixels to reduce capacitance. Indirect detection may also be practical, in which case there could be future opportunities to take advantage of large commercial developments of photodetector matrices. Evaporation of CsI(Tl) scintillators onto amorphous silicon diode arrays is an example of the possibilities (Drewer *et al* 1991) where in a prototype an array of 64 × 40 photodiodes was constructed, with each pixel containing a thin film transistor.

3.9.4. Diamond. Diamond, although not a semiconductor, has properties directly comparable to silicon. It is of interest because of a belief that it may prove to be faster and more radiation hard than silicon, and that developing industrial technologies, using chemical vapour deposition (CVD), could produce large detecting areas at low cost (Franklin *et al* 1992). Diamond is an insulator with a band gap of 5.5 eV and resistivity in the range 10^{11}–10^{16} Ω cm, and a high electric field can be applied with minimal dark current. However the large band gap compared to silicon requires more energy to produce each electron–hole pair. Although the density of diamond is higher than silicon the lower atomic number, longer radiation length and higher carrier mobilities in crystalline material are attractive features. Minimum ionizing particle signals have been observed in diamond detectors with effective charge collection thicknesses of up to 50 μm in CVD material.

4. Readout electronics

4.1. Noise in detector systems

Silicon detectors are normally operated well below the threshold for avalanche multiplication of carriers and do not provide any intrinsic amplification. The external amplification of the small ionization signals produced in the detectors is therefore crucial to their operation, and the implementation in the last few years of amplifiers in integrated circuit form has been a major step forward. This has come about in a number of stages, beginning with a thorough understanding of the optimization of low noise detector-amplifier systems (Nicholson 1974, Gatti and Manfredi 1986, Radeka 1988).

Noise in detector–amplifier systems is categorized as parallel or series noise to distinguish its electrical association with the amplifier input. The major noise sources in semiconductor detector–amplifier systems are shot noise from detector leakage currents and noise associated with biasing networks, which are both parallel sources, and series noise associated with the amplifier itself. The crucial element of a low noise system is the input stage of the preamplifier, and normally the first transistor. The most common amplifier configuration is the charge sensitive type, for its superior noise performance, although the current sensitive mode is sometimes used where speed is required and not minimum noise. The signal pulse is shaped into one of a number of standard forms, determined by practical considerations, to limit the bandwidth of signal and noise and optimize the signal to noise ratio.

In situations where parallel noise dominates there is no alternative except to use a short time constant system. Amplifier noise depends on the transistor technology: bipolar or field effect (MOS, Junction or MES). Bipolar amplifiers give their best performance

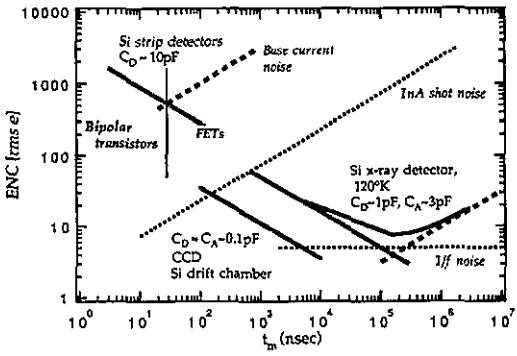

Figure 4.1. Typical values of the equivalent noise charge and their origins in some systems of interest as a function of time constant, t_m, which represents the characteristic peaking time of a unipolar pulse shaping filter (after Radeka 1988). Noise originating in parallel sources increases as $t_m^{1/2}$ while amplifier noise $\sim t_m^{-1/2}$

with fast pulse shaping since the series and parallel noise sources are both related to operating current in the transistor. The correlation causes a minimum at short time constants and only at time constants of order 10 ns do bipolar amplifiers match or improve on other technologies (figure 4.1).

Series noise in field effect transistors has two components: thermal and so-called $1/f$ noise, which is related to the surface of the device. Thermal noise is largely determined by the transconductance of the device and depends strongly on current. $1/f$ noise is minimal in JFETs, where the current carriers are transported away from the surface, but is considerably more important in MOS devices. Nevertheless in the range of time constants of interest (some ns–μs) for semiconductor tracking detectors, thermal noise usually remains the dominant noise source. JFETs are the input devices of choice in low noise amplifiers but optimal performance is obtained at long time constants when leakage current noise is not significant. They are therefore most widely used in spectroscopic systems and cooling the detector and the input transistor ensures superior performance.

4.2. Discrete component amplifiers

The development of semiconductor γ-ray spectroscopy systems in the 1960s and discrete JFET amplifiers (Kandiah 1979) led to detailed analysis of the optimal methods of signal processing under a wide range of experimental constraints (Radeka 1968). During this era amplifiers were usually constructed from discrete components on shielded printed circuit boards in a rather bulky form which was quite adequate for the read out of single elements. Gaseous position sensitive detectors of the 1970s were often based on interpolating techniques using delay lines or resistive electrodes so that only small numbers of amplifiers were needed. Multiwire proportional chambers could require many amplifiers but configurations could still be found which minimized the electronics at the detector (Radeka 1974). However during this period the electronics industry was developing smaller packages for components which were essential for the evolution of higher density detector systems.

The earliest experiments to read out large numbers of microstrips were able to instrument several thousand detector elements in an acceptably small space by producing amplifiers in thick film hybrid technology using discrete surface mounted transistors

(Manfredi 1983, Goyot and Jarron 1984, Alberganti *et al* 1986). The amplifiers were positioned at the end of multi-way cables which transmitted the current signals from the detector (figure 4.2(a)), usually via large printed circuit board or polyimide film 'fanouts' on which metallized, gold-plated traces coupled the high density microstrips (typical pitch 50 μm) to standard, commercial connectors (typical pitch 0.1 in). Apart from the extra capacitance associated with the connecting lines, with disadvantages for noise and electrical pickup, such a system was quite bulky despite the compact form of the amplifiers themselves (figure 4.2(b)). While this was acceptable for fixed target experiments where extra material introduced by the amplifiers, connectors and cables could be kept out of the sensitive region of the experiment, it was evident that colliding beam experiments required further miniaturization of the electronics in the form of integrated circuits.

4.3. Integrated circuit amplifiers

The most frequently used integrated circuits are based on MOS technologies, of which CMOS is now pre-eminent because of accessibility and the low power consumption possible in digital circuits at low and intermediate switching speeds. However the power consumption in amplifiers is usually still dominated by the requirements to minimize thermal noise in the input stage.

4.3.1. Switched capacitor circuits. The Microplex chip (Walker *et al* 1984) was the first of a series of chips which solved the problem of high channel density readout. It was a 128 channel circuit built using 5 μm NMOS technology in an area of 34 mm^2. A schematic of a later variant of the circuit (MX3) is shown in figure 4.3. Each channel consists of a charge sensitive amplifier followed by sample and hold circuits in the form of a pair of capacitors and associated transistor switches. The synchronous nature of colliding beam experiments is crucial to the operation of the circuit which uses a double correlated sampling technique by storing the output voltage of the integrating amplifier before and after a beam crossing. The difference between the two voltages is proportional to the charge deposited and allows the subtraction of switching transients, which should be identical for the two storage elements, and suppresses low frequency noise from the circuit with periods much longer than the interval between the switching times. The signal voltage is measured by a differential amplifier, with each channel on the chip sequentially connected to a single output line via a shift register. Multiplexing levels are determined by the time permitted for readout of the entire detector; usually, by connecting serially adjacent chips, it is around 10^3 channels per readout line.

A major innovation in the design of the Microplex circuit and several of its successors in CMOS technology was the use of switched capacitor techniques. These are natural techniques in monolithic MOS circuit design where capacitor ratios can be defined with great precision but precise value resistors and capacitors are less simple. For this reason the pulse shaping techniques of noise reduction could not be easily applied in monolithic circuits. A series of chips, of varying readout density, have been developed for experiments at e^+e^- and proton colliders and are summarized in table 2 (Schwarz 1992). They illustrate the evolution of power and feature size which has occurred in recent years; typical linewidths of processes in use at present are approaching 1 μm. The replacement of NMOS technology by CMOS allowed a substantial power reduction because, at the event rates encountered at present accelerators, maximum clock speeds of a few MHz are used. The radiation tolerance required of electronics in the e^+e^- environment is up

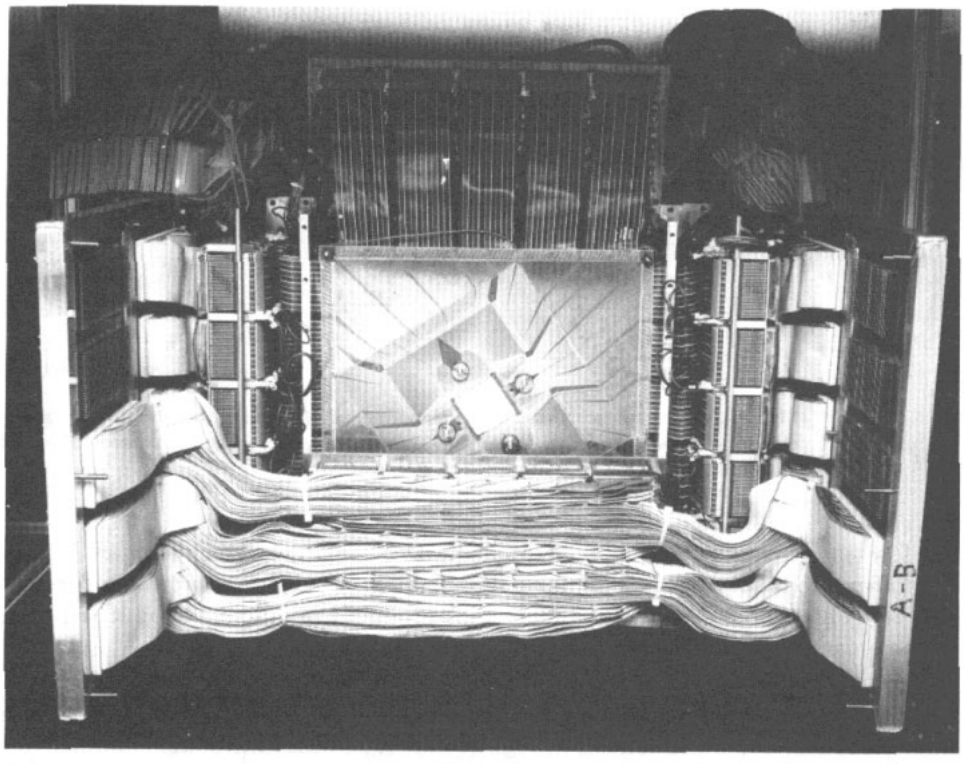

(*a*)

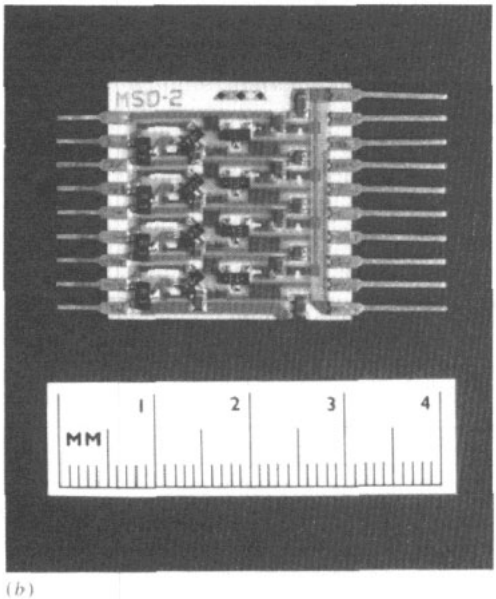

(*b*)

Figure 4.2. (*a*) The fixed target microstrip telescope and readout electronics used in the NA14 experiment at CERN in the mid 1980s. (*b*) One of the four channel thick film hybrid amplifiers (photographs N Jackson, Imperial College).

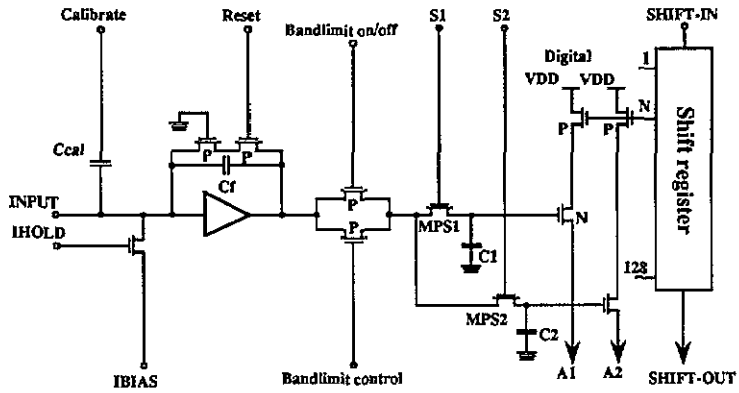

Figure 4.3. A circuit schematic of the MX3 amplifier. C1 and C2 are the storage capacitors used for the double correlated sampling. Transistor switches S1 and S2 control the operation sequence.

to a few tens of krad, which has been reached with non-hardened technologies. However, it is difficult to make firm statements on the hardness of individual circuits as substantial variations have been observed between chips produced in different production batches from conventional processes.

4.3.2. Time invariant filters. In switched capacitor charge sensitive amplifiers the first stage feedback loop must be reset at regular intervals, which introduces another source of noise from switching transients. As it is repetitive, it can be subtracted by correlated sampling but coupling of clock signals is a difficult problem of switching circuits which manifests itself as common mode noise in the system. For this reason, a passive resistor-like device in the feedback circuit is often preferred to allow the stored signal charge to decay away in a well defined fashion. This was implemented in an integrated circuit amplifier in the Amplex chip (Beuville *et al* 1990) by using a long channel FET with the gate biased to set the resistor value. The FET noise is below that of an equivalent value resistor because the thermal noise in the channel is determined by the drain-source current and not by the magnitude of the resistance. It also has the advantage that asynchronous systems can be instrumented, in which advance knowledge of the imminent arrival of a possible signal is not necessary, unlike the use of correlated sampling. Several amplifiers have since been built making use of this method, some of which

Table 2. after Schwarz (1992).

	Mark II	Delphi	Aleph	Opal	CDF
Chip name	Microplex	MX3	CAMEX64A	MX5	SVXD
Reference	Walker (1984)	Stanton (1989) Bingefors (1993b)	Buttler (1988)	Allport (1993)	Kleinfelder (1988)
Technology	5 μm NMOS	3 μm CMOS	3.5 μm CMOS	1.5 μm CMOS	3 μm CMOS
No. channels	128	128	64	128	128
Area (mm^2)	6.3 × 5.4	6.4 × 6.9	6.4 × 5.0	6.3 × 6.7	6.3 × 6.8
Bond pitch (μm)	47.5	44	100	44	48
ENC(e) (C_{in} in pF)	$280 + 97C_{in}$	$670 + 55C_{in}$	$335 + 35C_{in}$	$325 + 23C_{in}$	$350 + 58C_{in}$
Power/channel (mW)	~14	~0.5	~1	~2	~1.3

achieve the lowest noise performance using integrated circuit amplifiers reported to date (Nygård *et al* 1991, Aspell *et al* 1992).

4.4. High speed radiation hard electronics

Further hadron collider applications, in which interaction rates of 40 MHz will be typical, test the use of integrated circuit technology in further ways. It will be necessary to identify the time origin of events with the precision of a single beam crossing interval so fast pulses are mandatory. Low power readout is necessary because of the large number of tracking system elements, up to 10^7, but it is extremely challenging to process signals with low noise and low power using very short amplifier shaping times. In addition, the large data volume, even at the low system occupancies of order 1% expected, requires a first level of data reduction by a factor of order 10^3 to be achieved before data are passed from the detectors.

Several front end designs have been investigated for silicon microstrip tracking applications which should meet the requirements. A bipolar amplifier is claimed to offer the best high speed performance (Spieler 1991, Dorfan 1993) for a given capacitive load and noise specification and is proposed for hadron collider experiments at the SSC. Addresses of strips giving pulse heights above a comparator threshold are stored in a local memory with a digital time value until the data are required. Time jitter on the comparator is controlled by a time over threshold circuit. The system necessitates chips in two different technologies, since the digital storage chip is most easily implemented in CMOS. An overall power consumption of 1-2 mW/channel is the goal.

Alternatives based entirely on CMOS technology are considered more promising at LHC, where developments of analogue pipeline memories (Olsen *et al* 1989, Möschen *et al* 1990, Horisberger and Pitzl 1993, Munday *et al* 1993, Brenner *et al* 1993b) form the basis for the systems. Signals from the input amplifier are sampled at the beam crossing frequency and stored in the pipeline which has a maximum delay limited by the size of the chip. One novel technique uses a digital signal processing algorithm implemented as a low power analogue signal processor to achieve the aim of fast pulse shaping (Gadomski *et al* 1992, Bingefors *et al* 1993b). To obtain a power of 1-2 mW/channel the shaping amplifier uses a relatively long shaping time, of 40-60 ns and the sampled pulse is deconvoluted by a simple switched capacitor filter to retrieve the initial signal impulse confined to a beam crossing interval.

All of the circuits required for the read out of tracking detectors at hadron colliders must be implemented in radiation hard technologies and much work is presently under way to characterize the limited number of custom radiation hard processes available (Ziock *et al* 1990, Tedja *et al* 1992, Bouvier *et al* 1993, Anghinolfi *et al* 1993a, Radeka *et al* 1993, Dentan *et al* 1993, Berberis *et al* 1993, Cesma *et al* 1993). Hardness levels of up to 10 Mrad and 10^{14} n cm^{-2} are required. Cost and reliability considerations limit the size of the chips and the functions to be implemented within the detector in the high radiation environment. For this reason there is great interest in adopting high speed optical fibre telecommunication technology to transfer data from the detector to the external data acquisition systems. Some fibre links based on passive modulation schemes are radiation hard and offer additional advantages of immunity to electrical noise and virtually no power consumption (Stefanini *et al* 1993).

5. Particle physics experimental applications

5.1. Experimental requirements

The most important characteristic of semiconductor tracking detectors is, of course, their accuracy. This is complemented by the high level of possible segmentation which ensures separation of nearby tracks in the congested region close to the event vertex and reduces errors in track recognition. However to take full advantage of the intrinsic performance of microstrip detectors and CCDs requires building systems in which it is necessary to take account of both the precision of the measurements and additional uncertainties generated by scattering of secondary decay products in the apparatus. In practice, the mechanical construction of the system is of very great importance in ensuring that the proposed spatial accuracy is attained. This requires careful engineering, especially in the colliding beam environment, to build stable structures using low mass materials with key components reduced below their usual thickness. Cooling, even of the heat loads in present detector systems, creates extra challenges and the large number of channels in future detectors will make this even more problematic. Alignment and calibration are also major items.

In experiments to date the major task has been to identify events in which there is a strong likelihood that the decay of a short lived particle took place. In the initial experimental design performance is estimated by some simple considerations (Damerell 1986). If a secondary track from a decay is extrapolated back towards the event interaction point, it usually misses the vertex and the distance of closest approach, the impact parameter, can be used as a means to indicate the presence of a decay. Individual decays should be drawn from an exponential distribution of lifetime values in the absence of experimental bias. The impact parameter is particularly useful for enhancing samples of heavy particle decays because, to a good approximation, its magnitude depends only on the mass and lifetime of the decaying particle. The precision with which it can be measured is determined by the geometrical layout and spatial resolution of the apparatus and the amount of material it contains. The geometrical component can be minimized by providing an accurate measurement very close to the decay point and at least one further measurement far away. The multiple scattering error is the cumulative sum of the random deviations arising from Coulomb scattering in each material layer traversed and depends inversely on the particle momentum.

Some of the principal experiments which exemplify major developments are surveyed below. The earliest uses of silicon tracking detectors were in fixed target experiments as so-called telescopes of several measurement layers. In recent years colliding beam experiments have dominated particle physics experimentation and detectors constructed in several cylindrical layers have become the norm. The requirements for detectors can be somewhat different because in colliding beam experiments a measurement of azimuthal position (at fixed radius) is often emphasised to determine momenta using the curvature of charged particle trajectories in a solenoidal magnetic field, whereas in fixed target experiments both orthogonal coordinates normal to the beam direction are of equal importance.

5.2. Fixed target applications

5.2.1. NA1. One of the first electronic experiments carried out to search for charmed particle decays was the NA1 experiment which made use of the FRAMM spectrometer

to reconstruct secondary particles (Amendolia *et al* 1980a, Albini *et al* 1982, Bellini *et al* 1982). The main objective was to observe coherent photoproduction of associated pairs of charmed mesons and an active silicon target of 40 circular detectors of 12 mm sensitive diameter was employed to observe the primary interaction point and decays. Thirty of the layers were manufactured by ion implantation and 10 using surface barrier technology. They were 300 μm thick and stacked 100 μm apart, with a capacitance of approximately 300 pF per layer, considerably larger than the 80 pF due to the silicon alone because of air gaps and edge effects. Amplifiers using 0.5 μs and 0.16 μs filters were developed to ensure low noise with large capacitance but also operate at the high rates required by the experiment in the high intensity photon beam. The expected multiplicity steps signalling decays were clearly observed and several hundred candidate decays were collected in the first experiment. However to measure the D° and $D^{\pm}$ lifetimes individually required clear identification of the specific final state in each event which was possible for some events using the spectrometer track reconstruction. This motivated some of the first construction of microstrip detectors for improved precision (Amendolia *et al* 1980*b*).

5.2.2. NA11. A spectrometer used by a CERN collaboration made some of the earliest use of both silicon microstrips and, later, CCDs in the NA11 and NA32 experiments (Bailey *et al* 1984, Damerell *et al* 1987). Six planes of microstrips were used to define the hadron beam which was incident on a copper target. Downstream of the target six further planes of microstrip detectors were used to measure the tracks of charged particles to distinguish primary interaction and decay products. The 20 μm strip pitch detectors were constructed in a university laboratory on 2 in diameter silicon wafers with a sensitive area of 24 mm × 36 mm. The number of readout elements was minimised by spacing the readout strips at 60 μm pitch in the centre of the detector and 120 μm pitch at the edges and interpolating using capacitive charge division (England *et al* 1981, Belau *et al* 1983). To ensure that all the strips were at a very similar potential to avoid field distortions a strip of amorphous silicon was sputtered over the strip surface of the detector.

The spatial resolution of microstrip detectors was very carefully studied in the experiment in magnetic fields up to 1.7T and the shift in the centroid of the observed charge distribution was measured for holes (Belau *et al* 1983). It was found to be consistent with expectations of transport phenomena under the Lorentz force which is determined by the Hall effect (Popovic 1991). In the same experiment one of the first measurements of radiation damage effects in microstrip detectors was made (Dietl *et al* 1987) by observing increases in leakage currents and the effects of field distortions in the beam counters which resulted from bulk damage to the silicon.

5.2.3. Other fixed target experiments. Other experiments during the same period were also equipped with silicon detector telescopes and accumulated large samples of charmed decays, produced with different beams (Barber *et al* 1987, Engels *et al* 1987, Anjos *et al* 1987). Detailed lifetime and production characteristic studies were made possible by the use of these telescopes which required extensive computer facilities to analyse fully the large data volumes.

An example of the performance achievable is provided by a recent high precision fixed target vertex detector telescope installed in the CERN experiment WA92 to search for beauty particle production (Adinolfi *et al* 1993). The very small cross section for B-meson production relative to the total hadronic cross section dictates the use of good

event selection based on impact distance criteria to limit the number of candidate events for close scrutiny. Detectors with a strip pitch of only 10 μm covering an active area of 5 mm × 5 mm were constructed and positioned close to the target, with the first of 16 planes at a distance of 1.2 mm downstream, followed by 13 planes spaced at further intervals of 1.2 mm. The last two planes are 12 mm further downstream so that the entire system contains 8192 channels in a volume of less than 0.8 cm^3. The detectors are constructed on 14 mm × 14 mm silicon chips with the remainder of the surface area used to fan out the detector strips to bonding pads on an 80 μm pitch. Most of the detectors are 300 μm thick but the first six planes were reduced to 150 μm to minimize multiple scattering. Analogue data are read out so that position measurement by a centre of gravity method can be used where each strip is weighted by the pulse height observed in a cluster, which is typically 1–2 strips wide in the thinner detectors. In a beam test of the telescope a spatial resolution of 3.1 μm was measured using data where signals were observed on a single strip. Where charge was shared between two strips a resolution of 1.8 μm was observed.

Another feature of silicon detectors that can be very useful is the ability to construct counters in unusual geometric shapes, to instrument a confined volume or for specific experimental reasons. An interesting example of this is provided by detectors constructed for high energy nucleus–nucleus collisions (Giubellino *et al* 1989) in the HELIOS experiment at CERN. A concentric annular geometry, with 60 mm diameter rings subdivided into azimuthal sectors, was used so that particle multiplicities, which are extremely high in heavy ion interactions, could be easily measured as a function of angular direction. The signals from each detecting element were measured with ADCs to provide energy measurements but were also discriminated and summed in fast logic electronics to provide a set of multiplicity triggers for the experiment.

5.3. Colliding beam experiments

5.3.1. Mark II. The first working vertex detector at an electron positron collider was the silicon microstrip detector installed in the Mark II experiment at the Stanford Linear Collider (Adolphsen *et al* 1992) which began operation in 1990. It contained 36 single sided detector modules with strips parallel to the beam, constructed for the first time on 10 cm diameter silicon wafers, in three cylindrical layers between radii of 26 mm and 44 mm. Each detector had 512 strips but the strip pitch was different in each layer, 25 μm, 29 μm and 33 μm, and they were fanned out on the wafer surface in the outer layers so that alternate strips could be bonded to the 47.5 μm pitch readout chip. They were DC coupled to the 18 432 channels of analogue read out electronics. The length of detectors in each layer was also different so that all three layers extended to a polar angle of 40°.

During the construction of the detector problems of low interstrip resistance were noted which reduced the strip to strip resistance from the normal 1–3MΩ to values sometimes as low as 10–100 Ω. This was traced to electrostatic surface charge build up caused by the packaging used for delivery which induced an accumulation of holes beneath the oxide connecting adjacent p-type strips. Similar problems have been noted with other detectors (Amidei *et al* 1993, Peisert 1992) and can sometimes be enhanced, for example, by external humidity (Laakso *et al* 1993). Attention is therefore usually given to external conditions and to surface coatings applied to detectors.

The detectors were connected to ceramic thick film hybrid circuits on which the readout electronics were mounted. A laminated flat kapton cable of 50 μm thickness

was used to supply each detector module with power, control and timing signals, and connect the multiplexed signal outputs to the external data acquisition system. The detector hybrids and electronics were placed beyond the active detector region so as not to contribute to multiple scattering.

The basis of the support structure was two semi-cylindrical beryllium shells constructed by electro-discharge machining. The strategy used to attain the required mechanical precision of the structure was to mount each detector with an accuracy of about 50 μm and rely on accurate alignment techniques to determine the relative position of modules to 2 μm. Two survey methods were developed to establish the internal alignment of the vertex detector prior to using tracks recorded during normal data taking to obtain the position relative to other sub-detectors of the tracking system. The first method was to survey optically each module during installation using a three-dimensional measuring microscope while the second made use of a collimated beam from an x-ray tube. Finally, during the operation of the experiment, the system was monitored using a commercial capacitive probe to sense displacements between the outer surface of the structure and copper ground pads mounted on the adjacent wire chamber support.

Results found during operation demonstrate that even these careful precautions were not adequate to avoid a probable movement during installation or during subsequent temperature cycling of the system. However, despite this, the average position resolution achieved was 7.1 μm per layer and an impact parameter error of 25 ± 5 μm, using $Z^0 \rightarrow$ lepton pair events.

5.3.2. SLD. The SLD experiment succeeded Mark II at the SLC in 1991 and the SLD vertex dector is the first colliding beam experiment to employ CCDs on a large scale in high energy physics (Damerell *et al* 1990, Agnew *et al* 1992). It contains 480 CCDs, with a total of 1.2×10^8 pixels arranged in four cylindrical layers from 29.5 mm to 41.5 mm radius (figure 5.1.). The CCDs are laid out in 60 linear ladders, each containing eight

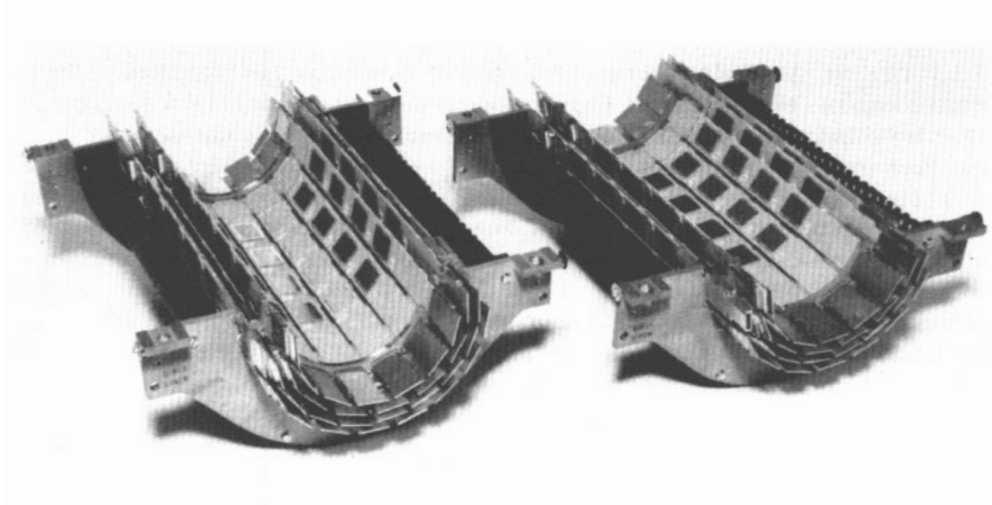

Figure 5.1. The upper and lower modules ofthe SLD CCD vertex detector prior to final assembly (Agnew *et al* 1992). The active length of each of the 60 ladders is 100 mm and the inner radius of the detector is 29.5 mm. (Photograph courtesy Rutherford Appleton Laboratory.)

CCDs of approximately 400×600 22 μm square pixels. Because of its proximity to the collision point the detector has excellent solid angle coverage and the very precise determination of both coordinates of tracks passing through it leads to powerful event reconstruction ability. The exceptional possibility to reconstruct short lived decays provided a strong motivation to undertake experiments of this kind at SLC.

A detector based on CCDs is possible at the SLC because of the peculiar beam structure of the accelerator which is a single pass linear collider, in contrast to circulating beam colliders. The machine operates at a bunch crossing frequency of only 120 Hz and this permits the long readout time of 160 ms required by the CCDs. The system is deadtime free as a second event during readout is registered since the detector remains continuously active; additional hits simply appear as background tracks originating from a second vertex in the event reconstruction. The probability of this type of occurrence is low; a more important background is from beam induced synchrotron radiation, accumulated over the 19 beam crossings during the readout period, which is spread randomly over the detector surfaces. However the high granularity of the CCDs allows this to be tolerated with negligible impact on the reconstruction of genuine tracks.

The total power consumption of only 12 W permits the detector to be maintained at -80 °C by passing a stream of cold nitrogen through the open spaces; it is housed in a foam cryostat. A special development effort was required to guarantee reliable miniature electrical connections to the low mass striplines during the thermal cycling of the equipment between operation. The mechanical support structure is machined from beryllium, chosen both for its mechanical stability and long radiation length. The CCDs were thinned, before being cut from the wafer, from an initial thickness of 580 μm to 200 μm. The effective total radiation length of the system, including beam pipe and cryostat, is 4% and tracks traverse, on average, 2.3 layers.

The spatial precision has been deduced to be 7.8 μm in the beam plane and 5.0 μm in the orthogonal plane from track reconstruction in the experiment. This remarkable result required an exhaustive optical survey of the detector, prior to assembly at the ladder level and after mounting in the semi-cylindrical barrels, both at room temperature and -80 °C.

5.3.3. DELPHI. At CERN silicon vertex detector technology was pioneered in the LEP experiments DELPHI and ALEPH. The microvertex detector installed in DELPHI (Anzivino *et al* 1988, Bingefors *et al* 1993a) has been operating since 1990, during which time it has been upgraded from its original design of two cylindrical layers to three (figure 5.2). The third and innermost layer was installed when the orginal aluminium beam pipe was replaced by one made of beryllium with a reduced radius of 53 mm. This allowed the possibility of adding a measurement point closer to the interaction point with reduced multiple scattering. The overall uncertainty of the impact distance measurement improved from $\sqrt{(80\,\mu\text{m})^2 + (120\,\mu\text{m}/p_t)^2}$ to $\sqrt{(24\,\mu\text{m})^2 + (69\,\mu\text{m}/p_t)^2}$ for tracks with transverse momentum, p_t, measured in GeV c^{-1}. This agrees with the value of 21 μm measured using 45 GeV c^{-1} muons from $Z^0 \rightarrow \mu^+\mu^-$ decays.

The three layers are positioned at radii of 63, 90 and 110 mm; they contain 288 detector wafers with a silicon surface area of 0.42 m^2 and 7.4×10^4 channels. The layers are of all the same length so each covers a different polar angular range, from 43° to 137°, while complete azimuthal coverage is ensured by overlapping the detectors by 10–15%. The system is constructed with single sided silicon microstrips, although plans are in motion to replace two of the layers with double sided detectors. At present the material in the active region contributes on average 1.5% of a radiation length. The

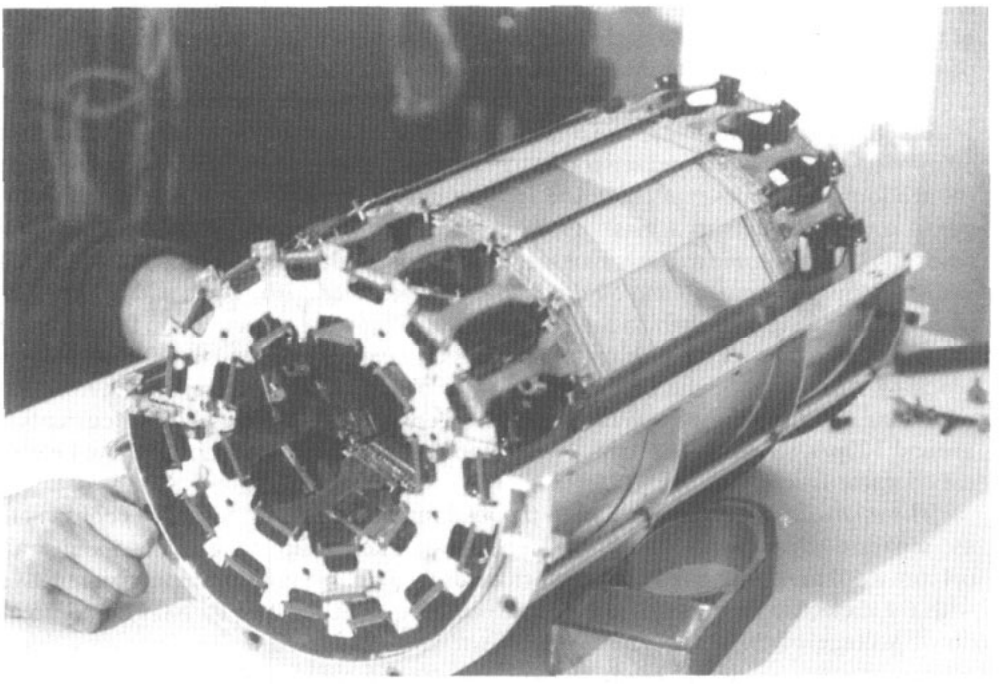

Figure 5.2. The ALEP minivertex detector assembled prior to installation in the experiment. (Photograph courtesy INFN Pisa.)

silicon detectors incorporate integrated coupling capacitors, using a 0.23 μm oxide layer on top of the strips, and polysilicon resistors, with values above 1 MΩ. The strips are laid out on a pitch of 25 μm but are read out at 50 μm intervals. Capacitive charge division is used to interpolate to find the centroid of charge clusters, using a non-linear algorithm which results in an average precision of around 8 μm over the entire detector, including angular effects.

The basic module of the system is a four detector unit constructed in two parts; each half consists of two silicon detectors bonded together and a ceramic readout hybrid at one end on which are mounted the MX3 128 channel amplifier chips. A profile constructed of 200 μm thick carbon fibre is glued to the back of each module for structural reinforcement with a narrow strip of 300 μm thick silicon glued to the other side to prevent bending caused by differential expansion. Two semi-cylindrical shells of the three detector layers mounted on aluminium end-rings were then constructed, with the detector modules themselves holding the two ends together, protected on inner and outer surfaces by a Rohacell foam layer. Cooling water flows in channels in the end rings to remove the 70 W dissipated by the electronics and stabilize the temperature to 0.3 °C. Two position monitoring systems, one based on capacitive probes, the other on a series of infra-red light beams focused onto the detector surfaces, measure any movements during operation. Overall alignment was based on an initial mechanical survey which established the relative position of each unit to 20 μm followed by alignment using measured particle tracks to a final precision of 5 μm.

5.3.4. ALEPH. The ALEPH microvertex detector was the first double sided silicon microstrip detector to be installed in a colliding beam experiment (Moser *et al* 1991, Batignani

et al 1993). Part of it was operated at LEP in 1990, with completion in 1991. It consists of two concentric layers of detectors at radii of 63 mm and 107 mm and contains 0.25 m^2 of silicon and 7.4×10^4 channels of electronics.

The 300 μm thick microstrip detectors are 51.2 mm × 51.2 mm, fabricated on 4 in wafers (Batignani *et al* 1991). The p^+ strips which measure the azimuthal co-ordinate are 50 mm long, 12 μm wide and separated by 13 μm gaps; every fourth strip is connected to the readout electronics, matching the 100 μm pitch. The strips terminate 5 μm from a guard ring which acts as a bias line using the punch-through effect to create dynamic resistors. On the ohmic surface, measuring the coordinate in the beam direction, 12 μm wide n^+ strips are implanted at 50 μm pitch and alternated with 12 μm wide p^+ implants acting as blocking strips which are left unbiased. When the detectors are fully depleted the p^+ strips interrupt the electron accumulation layer. At the ends of the detector the blocking strips confine the accumulation layer electrons into channels to the bias line which creates resistors of several MΩ after depletion. Very low leakage currents of around 120pA/strip, or 4 nA cm^{-2}, were reported, with high yield and excellent electrical characteristics.

The microstrips are AC coupled to the readout electronics by capacitors constructed as separate chips with 64 nm oxide layers. Each chip is a quartz substrate, 6.4 mm × 5.0 mm, with 64 capacitors formed using a double polysilicon layer interleaved with the dielectric from the oxide layers to achieve a capacitance of 200 pF and breakdown voltage of 20 V. The low breakdown voltage caused a few problems during operation when accidental beam loss into the experiment caused momentary high currents to flow in detectors and in some capacitors led to failure. However the advantage gained was a relatively simpler design for the double sided detectors than those with integrated capacitors. The consequent higher production yield reduced cost at the expense of doubling the number of bonds required. This was tolerable because of automation of the wire bonding process.

The mechanical assembly was a construction of four silicon wafers glued to a ceramic, and fastened to a lightweight graphite frame (figure 5.3). Detectors were bonded

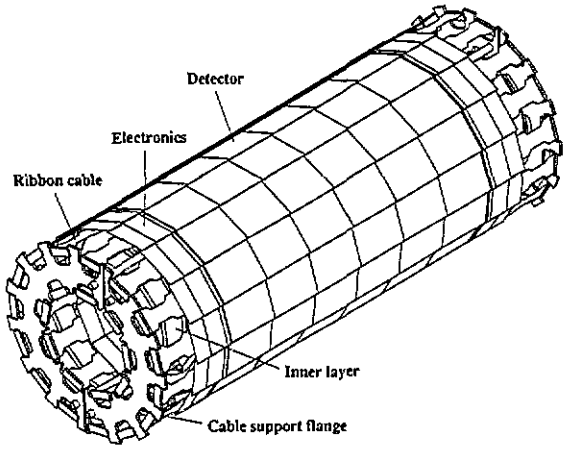

Figure 5.3. A three-dimensional view of the mechanical support structure of the upgraded Aleph minivertex detector due to be installed in 1995. The detector is constructed in two separate halves which are locked together on assembly around the beam pipe. The two detector layers are supported on two flanges not visible in the drawing.

together to create double length modules. The total power dissipation of 60 W was cooled by forced air which led to some problems when liquid residue from bubbles in epoxy used to protect wire bonds was deposited by the air stream on line driver chips and caused some failures. The structure was aligned in two stages; by optical measurement and using data from tracks in the experiment, achieving a resolution of 12 μm in both coordinates at normal incidence. An impact parameter resolution of 25 μm (in ϕ) and 29 μm (z) was the result.

5.3.5. OPAL. OPAL was the third LEP experiment to be equipped with a silicon microstrip vertex detector (Allport *et al* 1993). It was commissioned for data taking in 1991, having been installed very rapidly and clearly benefited from experience gained during the developments for Aleph and Delphi.

Because of the limited space available between the 53 mm radius beryllium beam pipe and the high precision gaseous drift chamber, the detector consists of two cylindrical layers at 61 mm and 75 mm. Each layer consists of six single sided microstrip detectors bonded together serially in units of three and read out at each end; the overall length of each unit is 180 mm. The detector modules are mounted on polygonal aluminium rings mounted inside a carbon fibre pressure vessel which seals the high pressure volume of the outer gaseous detectors. Power is removed by water cooling.

The 629 capacitively coupled read out strips of each detector module are spaced at 50 μm pitch; intermediate strips are provided at 25 μm spacing to allow charge division interpolation. Aluminium tracks on glass substrates are used to convert the 50 μm detector readout pitch to the 44 μm of the electronics. The detectors incorporate FOXFET structures (Allport *et al* 1991) to bias the individual strips with the operating gate voltage chosen to achieve a dynamic resistance of 10–40 MΩ, which then permits a signal to noise ratio 22:1 for minimum ionizing particles in the experiment. Test beam studies estimated an intrinsic detector spatial resolution of about 6 μm, which translates into an impact parameter resolution of about 18 μm in the experiment, measured with Z^0 di-lepton events.

5.3.6. CDF. The CDF vertex detector at the Fermilab Tevatron proton–proton collider was the first to be installed in a hadron collider experiment (Carithers *et al* 1989, Amidei *et al* 1993). It has been operating since 1992. It consists of four layers of single sided 55 μm and 60 μm pitch microstrip detectors between radii of 27 mm and 42 mm. Ladders of 510 mm length were constructed as two modules of three detectors with electronics at each end. They are mounted on a lightweight Rohacell foam support reinforced with carbon fibre strips. The ladders in each layer are of different widths to simplify the mechanical construction, varying from 256 channel units on the innermost layer to 784 channel units on the outermost. There are 4.6×10^4, water cooled, channels dissipating ~100 W and the whole system operates inside the argon-ethane gas volume of the surrounding wire chamber detector.

The electronics is based on the SVX chip (Kleinfelder *et al* 1988) which is a 128 channel switched capacitor chip with charge sensitive amplifiers, sample and hold circuitry and comparator and latch for each channel. It makes use of quadruple correlated, rather than double correlated, sampling to subtract the effects of leakage current in the DC coupled microstrips. A novel feature, compared to other systems in use, is the possibility of on-chip data suppression. Data can be read out in three modes: all channels, only channels above a given threshold, or channels above threshold plus nearest neighbour strips. In each case pulse height information is retained. The system

is subdivided for readout into 30° sectors which contain 1920 channels. Two thresholds are available for each sector, one for the inner layer, where the hit density is greatest, and one for the outer layers. This permits an occupancy of up to 20% while ensuring the total time for readout does not exceed the 2.1 ms available.

Threshold uniformity throughout the system determines the occupancy and particle detection efficiency since only a limited number of thresholds is practical. In the early stages of operation occupancy was maintained at 5–6%, increasing later to 15–20% as radiation damage increased noise on the inner layer. In addition, leakage current increases were observed in some ladders of the system, attributed to surface effects possibly related to the operation in the unusual gas mixture. At present, by maintaining the detectors constantly under full operating bias, satisfactory performance has been maintained.

5.3.7. L3. The L3 experiment is the most recent of the four LEP experiments to be equipped with a silicon vertex detector. Two concentric layers were installed for 1993 data taking (Adriani *et al* 1993). The double sided detectors are identical to those used in Aleph, with improvements in the design of the external quartz coupling capacitors to incorporate protection against the voltage spikes which can be induced in the system by beam losses into the detectors. Kapton printed circuit foils glued to the ohmic surface of the detector will permit the readout electronics to be based at the end of the system with minimal extra material in the active region by coupling the orthogonal n-side strips to metal traces parallel to the p-side surface. The readout is based on SVX chips produced in a radiation hard technology. Various levels of data suppression can be applied, with analogue data digitized 10 m from the detector and transferred from the experiment on optical fibre links. The support structure is based on a carbon fibre composite with cooling by chilled water supplemented by dry air.

5.4. Other experiments

The ability to construct highly segmented, precise systems in small volumes is an important feature of silicon based tracking systems. In many experimental environments this is an indispensable prerequisite of important physics studies. B particle production at hadron colliders and e^+e^- B meson factories are good examples, where the majority of events are produced in a region close to the beam line and compact instrumentation is essential. A prototype system of 4.3×10^4 channels has been demonstrated (Ellett *et al* 1991) in the P238 experiment where silicon microstrip detectors were mounted in vacuum vessels integrated into the CERN SPS machine beam pipe so that the detectors could be positioned only 1.5 mm from the circulating proton and antiproton beams. They could be retracted during beam manipulations to a distance of at least 50 mm. The Roman Pot system, which incorporated a corrugated aluminium window 200 μm thick, allowed operation free of RF interference despite the close proximity to the beams.

This summary cannot do justice to the large number of experiments equipped with silicon tracking detectors and the innovative solutions found to specific problems. The reader is invited to consult the literature for details.

6. Non-particle-physics applications

Most of the applications of semiconductor detectors outside the field of nuclear and particle physics are in the area of x-ray detection. In the low energy regime of 0.1–

10 keV, which is of great interest to astronomers, the use of silicon CCDs is one of the well established competing techniques (Culhane 1991, Wells and Pounds 1993) where both spatial and energy resolution are required. Although the energy resolution is excellent, one of the limitations is the thin active volume and the absorption in gate structures and insulating layers on the surface of the device. This has motivated modifications to conventional CCDs and developments of p-n junction CCDs discussed later. However, apart from the proposed detection of ultra-high energy electromagnetic showers using silicon strip devices in a balloon borne calorimeter (Bocciolini *et al* 1987), other presently available semiconductor detectors have not been widely considered. Small element sizes are necessary to achieve the good energy resolving power required in low energy x-ray detection and few other devices can match the performance of the CCD.

Similar considerations hold in the areas of x-ray imaging for biology and medicine, although a wider energy range is covered (Faruqui 1991). Semiconductor and gaseous detectors are among several types of position sensitive detectors of interest for measurement of protein diffraction patterns and absorption spectroscopy (Fontaine 1987); CCDs have been mainly used as integrating visible photon detectors in combination with converting phosphors. An electronically collimated gamma camera (Singh and Doria 1983) is one method which could reduce patient exposures in clinical diagnoses if suitable detectors were available; studies suggest this would be feasible using microstrip technology (Solomon and Ott 1988).

At present the drawbacks of solid state detectors are the small areas covered. In other respects they offer superior performance to x-ray film in linearity, dynamic range and sensitivity. They offer the possibility of faster image production and off-line image processing as well as time resolved studies but to realise these gains requires an investment in technology and effort that small scale applications are usually unable to provide. Therefore spin-offs from particle physics detectors have been a source of some initiatives (Alfano *et al* 1992, Rönnquist *et al* 1993) where silicon microstrip detectors have been investigated for x-ray detection and higher Z materials have been considered as a means of increasing the range of energy sensitivity (Benvicelli *et al* 1991). The pixel detectors currently under development for particle physics experiments may be an example of a technique which is widely applicable outside the field (Raymond *et al* 1991) and detectors based on silicon appear to have attractive features for x-ray detection at high rate synchrotron sources (Hall 1992, Warburton *et al* 1993) provided a way is found of covering modest size areas with minimal dead regions.

7. Current developments

7.1. Future hadron colliders

The stage for particle physics experiments is planned to shift from electron-positron colliders to high intensity proton-proton machines at the end of the century. The Standard Model of particle physics interactions has been under intense study in e^+e^- collisions, particularly at the CERN LEP machine, and has been found to be in impressive agreement with experiment (Marciano 1991). Nevertheless, at energy scales approaching 1 TeV the Standard Model is expected to be inadequate and the significance of some empirically defined parameters may become evident. In addition, symmetry breaking in the theory should be explained by the existence of a scalar particle called

the Higgs boson whose mass is not precisely predicted but which is expected to be found in the energy range of new proton colliders. The Large Hadron Collider (LHC) is being planned at CERN and, until recently, the Superconducting Supercollider (SSC) was being built in the USA. However the production rate of the Higgs, and other exotic particles, is so low that experiments are only feasible if the machine operates with extremely high luminosity. This is achieved by circulating intense proton beams which undergo collisions between counter-rotating bunches every 15–25 ns.

At maximum LHC luminosity, 10–20 interactions occur in every beam crossing producing several hundred secondary particles. The flux of secondary particles is so high that 1 Mrad radiation doses each year of operation are expected for the innermost detectors. The charged particle dose decreases inversely with the square of radial distance from the beam but is accompanied by a roughly isotropic flux of fast (~1 MeV) neutrons which have their origin in the collisions between outgoing charged particles and the dense calorimetric detectors surrounding the central detector volume. The experiments which are being designed plan to instrument the interior region with tracking detectors; some are intended to operate with high efficiency for many years of high luminosity operation during which integrated doses of 10 Mrad and 10^{14} n cm^{-2} will accumulate. Despite these hostile conditions, semiconductor detectors are among the most promising candidates for the SSC and LHC tracking environments, and the only means of making accurate spatial measurements in the vicinity of the beam. Intense R&D is under way with the goal of instrumenting experiments with radiation hard, high speed and high performance detector systems. Silicon and gallium arsenide detectors both offer high speed charge collection, which is maintained after LHC type radiation levels, although silicon is certain to be more widely used than any other material because of the mature technologies available for detector and electronics fabrication.

7.2. Radiation damage to silicon detectors

The major effects which have been oberserved to take place in silicon after high levels of irradiation fall into two classes, reviewed by Gover and Srour (1985), Messenger and Ash (1986), Ma and Dressendorfer (1988) and Holmes-Siedle and Adams (1993). Surface damage gives rise to inter-band gap energy levels and mobile surface states with a range of time constants. An important phenomenon observed is an increase in the density of short time constant traps and positive charge fixed in the oxide close to the silicon-oxide interface; the magnitude depends on several parameters including the oxide field. In MOS devices the results are increased surface leakage currents and transistor threshold voltage shifts. Surface damage effects have been investigated for many years for military and space electronic applications and radiation hardened technologies have evolved which can provide long term operation at LHC and SSC. Many process techniques could not easily be applied to detector fabrication, partly because of strategic and commercial importance and the consequent reluctance of manufacturers to describe them openly. However, surface effects are not the main obstacle to silicon detector operation at proton colliders; bulk effects are of much greater importance.

High energy particles crossing crystalline layers occasionally displace atoms from their lattice positions. In silicon only about 15 eV is required for this and the recoil of an atom with significant kinetic energy is quite commonplace. The simplest defects which result are vacancies, where a silicon atom is absent from its site, and interstitials, where an atom occupies a position intermediate between other atomic sites. Fast recoiling atoms initially lose energy mainly by ionization but as they slow to below about

30 keV kinetic energy they displace more atoms and create clusters of disordered regions a few hundred Å in linear dimensions. Most clusters are unstable, since at room temperature the simplest defects are mobile until they become trapped at a surface or other energetically favourable location. These processes lead to a gradual reordering of the crystal, some of which occurs over long periods of time, during which stable defects form.

Disruption of the symmetry of the crystal, which is the basis of semiconductor properties, causes the formation of energy levels in the normally forbidden region between the valence and conduction bands. Unwanted energy levels have several serious consequences, the most evident of which is an increase of leakage currents. The presence of energy levels close to the centre of the band gap considerably enhances recombination-generation currents and measurements have demonstrated that these are the main source of dark current in radiation damaged detectors. The volume current density is observed to increase linearly with particle fluence (ϕ) for heavy particles, with $\Delta I/V = \alpha\phi$.

The damage constant (α) is approximately 8×10^{-17} A cm^{-1} for fast neutrons, once self annealing, temperature and incident energy corrections are made (Gill *et al* 1992, Fretwurst *et al* 1993). Recent measurements also appear to confirm the validity of a relation between non-ionizing energy loss and damage by different types of particle (Van Ginneken 1989, Huhtinen and Aarnio 1993), first conjectured in connection with electronic devices, so that high energy charged particles probably give rise to similar damage to fast neutrons, although the data are at present less comprehensive.

The defects which increase leakage currents are not well identified, although some common ones have been isolated in a number of studies (Heijne 1983, Wunstorf *et al* 1990, Bruzzi *et al* 1993). Other complex defects are needed to explain significant changes in the silicon substrate doping levels which at present appear to provide the ultimate limit to detector lifetimes. Because of the relative lack of commercial interest in the ultra-high resistivity material used for detectors, these effects do not appear to have been widely studied in the past.

High resistivity detector grade material, of both p and n-type, contains roughly equal numbers of acceptor and donor atoms with the imbalance between them determining the substrate type. Observations over many years (Konozenko *et al* 1971, Sigfridson and Lindström 1976, Heijne 1983, Gill *et al* 1992, Pitzl *et al* 1992, Ziock *et al* 1993) have demonstrated dopant density changes during irradiation. The effect is poorly understood, in terms of elementary defects, but has been parametrized in a simple model of donor removal whose rate is proportional to donor density accompanied by a constant rate of acceptor creation. This leads to a parametrization of the form (Fretwurst *et al* 1993) of the doping concentration, $N_{\text{effective}}$, after a particle fluence ϕ

$$N_{\text{effective}} = N_{\text{D}} e^{-a\phi} - N_{\text{A}} - b\phi$$

where N_{D} and N_{A} are the donor and acceptor concentrations prior to irradiation. This describes most of the available data rather well (figure 7.1), although the underlying physics is not well established and awaits detailed semiconductor simulation using observed energy levels. Since the substrate eventually becomes p-type, whatever the initial type or resistivity, with increasing particle fluence the depletion voltage of the detector increases without limit. Although partially depleted detectors can be operated, charge collection in the undepleted volume is slow and occurs with reduced efficiency if traps are present so signal degradation is eventually inevitable. Operation is probably practical to fluences beyond 10^{14} cm^{-2}.

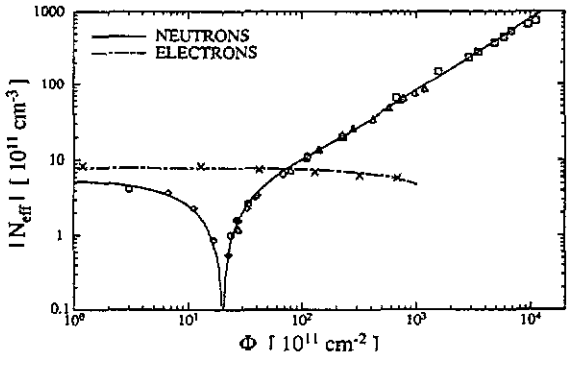

(a)

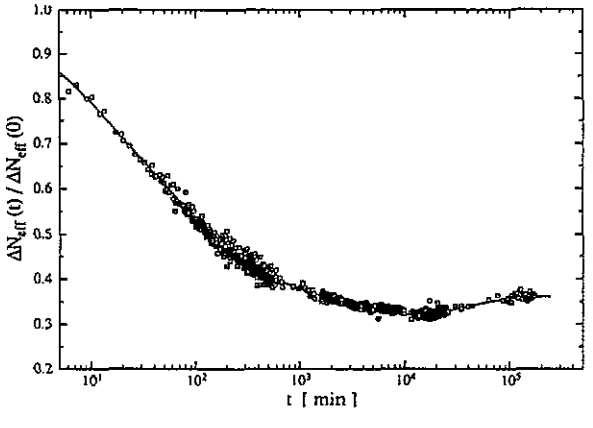

(b)

Figure 7.1. (*a*) Absolute value of effective doping concentration vs fluence of neutrons and electrons (Fretwurst *et al* 1993). It should be noted that the data are corrected for short term annealing. (*b*) The effective doping concentration compared to its pre-irradiation level following neutron irradiation. During the first few days room temperature self-annealing repairs some crystal damage. Longer term annealing leads to further creation of acceptor states at room temperature which ultimately limits operation in high particle fluxes.

These observations provide a principal motivation for interest in other materials, especially gallium arsenide, where encouraging measurements have been made on highly irradiated detectors (Beaumont *et al* 1993). Gallium arsenide detectors show minor increases in leakage current after extremely large particle fluences and signals have been observed up to fluences of 10^{15} n cm^{-2}, although degraded in quality. This is because the substrate material is already heavily populated with intermediate levels in the band gap and radiation induced levels do not dominate, unlike silicon. However there is some way to go before fully efficient large area microstrip type detectors can be produced. In the meantime there are some hopes that further improvement in the radiation hardness of silicon detectors might be achieved, once the basic damage mechanisms are fully understood.

7.3. Pixel detectors

The second major area of current research also has roots in requirements for tracking detectors at the SSC and LHC machines, as many radiation damage problems can be

avoided with detectors of extremely small volume. Elementary diodes are easily produced in any size and it was appreciated early that diode arrays coupled to high density readout electronics offer advantages of excellent signal to noise ratio and optimal spatial information. The region close to the interaction point, where radiation doses are highest, and where high resolution measurements close to the interaction point are essential to reconstruct decays of short lived heavy flavour particles could be instrumented in this way.

The advantages of pixel detectors are not restricted to future hadron colliders but would be utilized at any machine where large numbers of heavy quark decays could be observed (Hallewell 1993). They also appear attractive for applications outside particle physics where true two-dimensional images are often required.

7.3.1. MOS and p–n CCDs. Pixel detectors may be loosely defined as semiconductor devices with large numbers of detecting elements laid out in a two-dimensional array. It is usual to have in mind elements of up to a few hundred microns on a side with integrated readout electronics incorporated into the structure of the detector. Until recently the only devices which qualified using this definition were CCDs. Although they proved to be detectors of remarkable utility in some particle physics experiments, they have some serious drawbacks for future applications. The sequential organization implies long readout times, impractical in many contexts, and the non-hardened MOS technology is normally quite sensitive to rather low radiation levels, 10–100 krad (Roy *et al* 1989, Holland 1993), although recent innovations in design expect to improve on this considerably (Wells 1993). Both reasons render currently available CCDs inconceivable for hadron collider applications. The thin detector region and consequent small signals, and need for cooling, add to their disadvantages.

Improved CCDs, with respect to tracking applications, are not ruled out; deep depletion devices on high resistivity silicon have been manufactured (Culhane 1991) and parallel readout structures have been considered. Another possible approach is to build CCDs of a different type (Strüder *et al* 1987), derived from the drift chamber concept. An n-type substrate is implanted with p-type dopants into both surfaces, creating a potential minimum for electrons deep within the wafer when biased to full depletion. By modifying the n-type doping under one surface the potential minimum can be shifted towards the oxide and form a channel for electrons to be steered towards the readout node. The n-type implant also prevents large currents being injected as surface electrodes are biased to different potentials during the readout sequence. The first tests of the concept (Strüder *et al* 1988) were made on a linear array of 33 pixels of dimensions 150 μm × 100 μm. Larger two-dimensional arrays have since been produced (Strüder *et al* 1990), initially with relatively low charge transfer efficiency. More recently 64 channel devices of 30 mm × 10 mm have been tested (Bräuninger *et al* 1993) with parallel readout of columns of 200 150 μm × 150 μm pixels. The noise level was typically 7 electrons RMS with a charge transfer efficiency of 0.992 when operated at 200 K at a transfer speed of 600 kHz, requiring 15 ms for full frame readout.

The object of the p–n CCD development is x-ray imaging in a satellite mission which requires high energy resolution at low x-ray energies. To achieve the noise performance proposed it is essential to integrate the front-end amplifier directly onto the detector to match the small capacitance of the readout node to the amplifier. This is achieved (Pinotti *et al* 1993) by incorporating a circular JFET in a source follower configuration close to the collection anode; with a shaping time of 5 μs a noise of 2 electrons is reached at 150 °K.

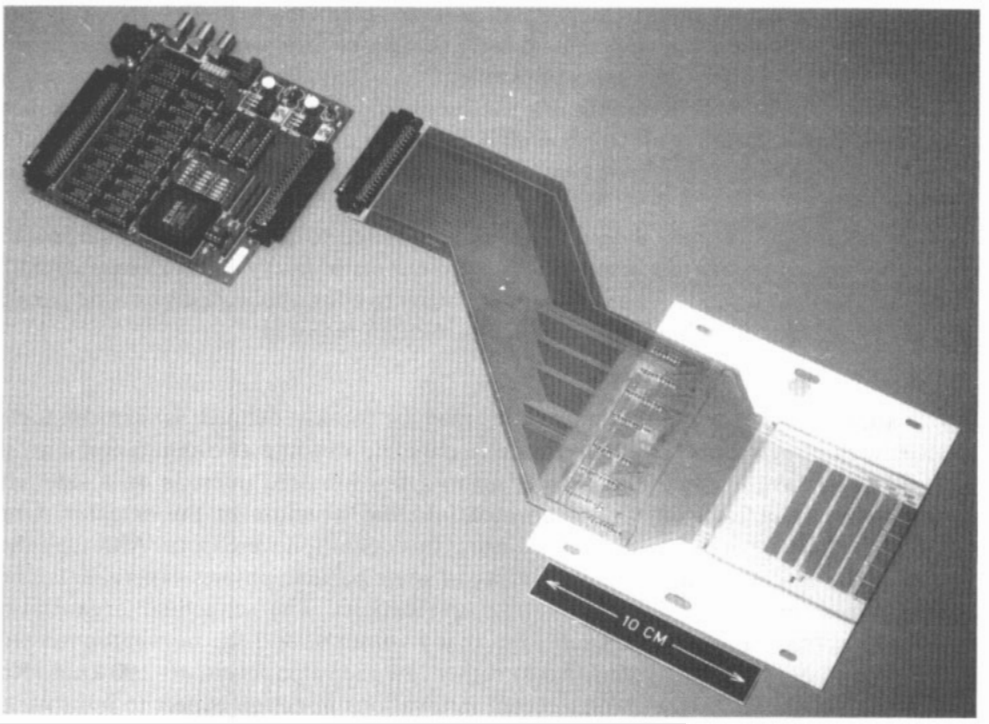

Figure 7.2. Some of the pixel detectors being developed by the RD19 project mounted on their readout ladders for use in beam tests (photograph courtesy CERN).

7.3.2. Hybrid pixel detectors. Alternatives to CCDs are currently being developed in two different ways: as hybrid or monolithic devices. The hybrid pixel detector consists of an array of detector diodes, laid out on a high resistivity substrate, and a separate, geometrically matching, array of electronic readout cells manufactured on low resistivity silicon in a separate fabrication process (figure 7.2). The advantage of this approach is the possibility to decouple the sensitive manufacture of the detector diodes from the electronics, which can therefore be optimized for speed and sensitivity in a standard commercial technology. The major potential difficulty is the high density interconnection between the detector and readout substrates, which has been demonstrated to be possible using bump bonding technology, developed in recent years in industry (Goldman and Totta 1983, Pedder 1988).

Several dedicated efforts are under way to produce hybrid pixel detectors, of which the most advanced is a development programme based at CERN (Anghinolfi *et al* 1993*b*). Pixel planes have been successfully tested in a fixed target experiment (Beker *et al* 1993) and high detector efficiency and good position measurement demonstrated. A telescope of three pixel detectors, each containing 1006 active pixels of area 500 μm $\times$ 75 μm laid out in 16 rows by 63 columns was installed in a sulphur ion beam incident on a sulphur target. Recently an array of detectors covering a total area of 25 cm^2 has been operated. Each pixel (Anghinolfi *et al* 1992) contains a charge sensitive preamplifier, comparator, delay and memory element allowing an entirely digital readout; the amplifier is directly coupled to the detector so the feedback loop incorporates leakage current compensation by subtracting the current sensed on a dummy pixel. The

signals are effectively shaped with a time constant around 50 ns prior to discrimination. The RMS noise level was estimated to be below 100 electrons on individual pixels but larger comparator threshold variations of ~750 electrons were observed across the array, attributed to normal manufacturing variations. The variation can be reduced by increasing the gain of the first stage although this may limit the range of signals which can be handled. For minimum ionising signals the performance is acceptable, even with thinner detectors than 300 μm silicon.

The maximum readout speed was 5 MHz in the test. Although this is somewhat lower than eventually expected it illustrates the need for careful design of the data handling logic to ensure that the high speed detection capability of the detector is not limited by the time required for overall readout of data from the array. Studies have been made of architectures which optimize the readout speed (Wright *et al* 1993) and schemes have been proposed which would allow the tagging of data from individual beam crossings at SSC and storage in pipeline memories.

Another pioneering development based in the USA (Shapiro *et al* 1989) connects existing readout arrays to silicon detectors by means of indium bonding, which has been applied to produce detectors for infra-red imaging applications (Arens *et al* 1987, Galeema 1989). The bonding process cold welds matching arrays of indium bumps under pressure to form low resistance contacts. Several silicon diode arrays of different cell sizes have been produced with up to 256×256 30 μm square pixels. Prototypes have been tested in a high energy pion beam (Shapiro *et al* 1990), achieving good signal to noise ratio.

For applications at the SSC the system would rely on the fact that the occupancy of high granularity detectors is very low so only a small number of pixels are hit in the same beam crossing interval. A global signal can be produced from an array when any element is hit. The signal charge from each cell is stored on the gate of a readout transistor and individual pixels are addressed by peripheral logic circuitry. If the array is hit, the beam crossing time is stored in a content addressable memory and hit pixel locations are stored in a random access memory. When a trigger signal arrives, elements corresponding to the time interval of interest are read out preserving the pulse height information. The pixels are then reset to receive future hits.

7.3.3. Monolithic pixel detectors. Monolithic pixel detectors envisage developing both electronics and detector elements on a single silicon wafer. Optimal matching of detector and readout elements may be possible without incurring any burden of stray capacitance and the complete device is as thin as the original wafer, although it is necessary to design the structure in such a way that electric fields still guarantee signal charge collection at the desired node of the circuit with no inactive regions. However, there are significant obstacles to be overcome to construct monolithic pixel detectors. The substrate must be a high resistivity wafer, to ensure that it can be depleted to a sufficient depth for adequate size signals, and there is a risk that subsequent electronic processing steps will have an adverse effect on the detector quality. A customized fabrication process must be developed to ensure that detectors and electronics are compatible and this may be a further barrier to producing radiation hard devices. Prototype amplifiers with good performance have been manufactured on high resistivity silicon (Radeka *et al* 1988, Holland and Spieler 1990), demonstrating the principle.

Despite the difficulties inherent in the monolithic approach, a working prototype with impressive performance demonstrated in beam tests has already been produced (Snoeys *et al* 1992, 1993). The original concept (Parker 1989) proposed to make use

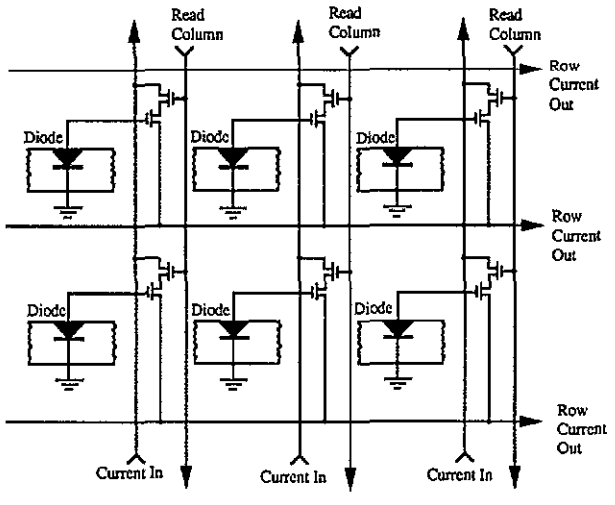

(a)

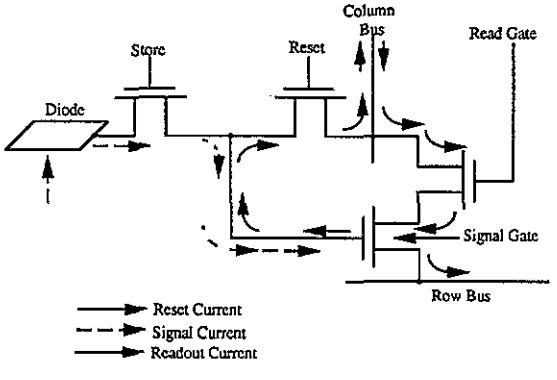

(b)

Figure 7.3. (*a*) A schematic of the monolithic pixel detector proposed by Parker (1989). (*b*) The sequence of signal integration and readout.

of the voltage produced by the ionization charge from a fully depleted detector deposited on a small detector capacitance (figure 7.3(a)). While in most microstrip detectors the typical voltage amplitude is in the sub-mV range, for pixel capacitances of ~0.1 pF a signal voltage capable of being measured without undue attention to noise can be produced. Small p–n diode detector elements are embedded into a matrix of electronics on high resistivity silicon and the presence of a signal voltage is sensed by connecting the diode to an MOS transistor gate. During readout each column of the array is turned on sequentially by a second transistor. The gate voltage applied by the signal controls current flow from a column bus to a row bus (figure 7.3(b)) and parallel measurement of the row currents determines the position of a hit pixel in the array at reasonably high speed.

The pixel arrays were fabricated in a 2 μm BiCMOS process on a 300 μm thick p-type substrate. The collection electrodes were provided by small area p-type contacts

in a large n-well and charges were stored on the gates of nearby PMOS transistors surrounding the ohmic contacts to the substrate. CMOS circuitry was implemented at the periphery of the n-well to control the readout sequence. Three hundred cells of 34 μm × 125 μm were produced in 30 rows and 10 columns. An n^+ diffusion produced the diode junction on the opposite surface to minimize electric fields in the vicinity of the electronics, so double sided wafer processing was required. However this allowed the exploitation of a polysilicon gettering technique (Holland 1989) developed for producing low leakage current detector structures in conventional integrated circuit processes.

The arrays were tested in the laboratory with a signal to noise performance for minimum ionizing signals of 150:1. In beam tests four planes of pixels were tested with somewhat higher noise but particle tracks were easily visible and the efficiency of individual pixels was consistent with 100%. Several pixels were usually hit in each event since charge frequently diffused on to more than one pixel. This allowed a non-linear interpolative technique to be used to improve position measurements and a resolution of 1.8 μm was achieved in the direction of smaller pixel dimension (Kenney *et al* 1993).

An attractive method for overcoming the need for a custom fabrication process for monolithic pixel detectors has been demonstrated recently (Dierickx *et al* 1993) by producing high resistivity silicon wafers with a buried insulating layer using a high energy oxygen implant (Simox) or zone melt recrystallization (ZMR). Both methods allow the production of silicon on insulator (SOI) circuits on the low resistivity silicon surface layer. The performance of detector test structures produced on the high resistivity substrate, after electronic processing steps had been carried out on the SOI upper layer, was excellent. So far, readout circuits have not been produced to instrument detector elements but MOSFETs and other simple circuit elements were fabricated successfully. The SOI technique may also offer a direct route to radiation hard monolithic pixel devices.

Another interesting concept which is still at an early stage of development is an integrated pixel detector based on an array of transistor-like structures providing both detection and amplifying functions (Kemmer and Lutz 1987). The DEPMOS (depleted p-channel MOS) device uses the drift chamber principle where a high resistivity substrate is fully depleted by biasing from both surfaces. As in the p-n CCD the electron potential minimum can be shifted towards one of the surfaces by applying appropriate voltages, in this case to a distance of a few μm from a surface oxide layer. The DEPMOS is laid out so that the oxide separates the source and drain of an active transistor and the arrival of a signal charge under the gate oxide modifies the transistor current, in a similar fashion to modulation by an external gate voltage.

Several prototype pixel elements have been constructed and tested. The design of the charge collection region was determined by simulation and the structures were constructed using an epitaxial n-type layer on an n-type substrate (Kemmer *et al* 1990, Lechner *et al* 1993). Since the amplifier and detector form part of the same structure the capacitance at the readout node is minimized, and non-destructive sensing of the signal is another advantageous feature.

8. Summary and conclusions

In the last decade semiconductor detectors for tracking in particle physics have matured rapidly from modest prototypes to large scale systems for colliding beam experiments

with $\sim 0.5\ m^2$ of detector area containing 10^4–10^5 channels in confined volumes with stringent constraints on power and mechanical construction. They are all based on silicon, which has become established as the principal material with which to construct tracking dectors because of the mature state of commercial fabrication technology. The detector developments seem to have fortuitously coincided with those in electronic fabrication in other ways: without integrated circuit readout, offering inexpensive prototyping, low unit production cost and high uniformity, the large systems now in use would not be feasible.

All of the colliding beam detectors constructed so far are complex systems, electrically and mechanically. Different compromises have been chosen between the many experimental requirements of high spatial precision, high density electronic readout with modest power dissipation, low mass construction, acceptable data volumes and long term reliability. However in each experiment the result has been a powerful detector making important contributions to the physics studies undertaken. Despite the apparent attractive features of some systems it is not possible to demonstrate overwhelming superiority of one set of technical choices; each experiment has been engineered for specific circumstances and their final performances are rather similar.

The electronic fabrication technology, which is a cornerstone of the construction of the particle detectors described here, is based on many years of a wide range of commercially motivated developments, from the basic physics of semiconductor materials and devices to technical innovations of connectors, circuit boards and components. Without this substantial foundation it is unlikely that the achievements of the last decade would have been so impressive. It remains to be seen whether the requirements for particle physics detectors using materials other than silicon will provide sufficient incentive for similar progress. In areas where the potential for improved performance, such as radiation hardness, has yet to be realised the evidence is still rather weak, and improvements in silicon detector performance have so far diminished the drive to invest heavily in gallium arsenide and diamond. Conversely, innovations for commercial reasons may provide further possibilities for detectors of the future where optical technologies appear to be of special interest.

The fertility of microelectronic technologies has attracted the interest of other detector physicists; gaseous microstrips (Oed 1988, Angelini *et al* 1989) are recent innovations in the already mature gaseous detector field. A metal coated glass plate is etched to construct strips which form anodes and cathodes on one surface and a few mm thickness of gas is sandwiched between the plate and a second cathode surface. A bias voltage of several hundred volts creates a sufficient electric field for gas gains of 10^3–10^4 to be achieved and generates signals similar in magnitude to silicon detectors which can be read out by identical amplifiers. The short distance between anode and cathode allows positive ions to be collected rapidly and thus provides fast signals while the high quality definition of the metal strips ensures uniform gain. A spatial resolution approaching that of semiconductor detectors (30–40 μm) is attainable under the most favourable circumstances and some of the limitations imposed by the size of available high resistivity silicon wafers are less stringent. Although not yet fully proven, they appear capable of providing the basis for instrumenting parts of the large experimental systems planned for the next decade and continue to inspire improvements of the basic concept (Angelini *et al* 1993).

Although new or upgraded detector systems are being constructed rapidly with increasing confidence, nevertheless there are major new challenges to be overcome. The tracking detectors proposed for the next experimental generation at new hadron colliders (SDC 1990, CMS 1992, ATLAS 1992, GEM 1992) will contain 10^6–10^7 electronic

channels and must be operated with high readout speeds in a radiation environment not previously encountered. Given the scale of these systems, there are new requirements for long term reliable operation with restricted access—which must be achieved at low unit cost. Microstrip technologies seem to be capable of meeting these goals but careful consideration of the complexity of the systems will be essential. It may be necessary to select the simpler system elements, in contrast to recent developments of more complex detectors.

The large scale use of CCD detectors in the SLD experiment has proven the power of pixel detectors for high energy physics and, among the many detectors developed for particle physics, these perhaps have the most relevance to applications outside the field. The principles of hybrid pixel detectors are now proven by existing prototypes. Future devices must be customized to allow the reduction of the large data volumes which can be registered by the detectors and much work remains to be done to define the electronic architectures capable of handling them.

Acknowledgments

I should like to thank many colleagues who have helped me by providing information and for valuable discussions on the contents of this paper, in particular P Allport, G Barber, D Barney, C Buttar, C Del Papa, L Evensen, E Focardi, E Fretwurst, C Haber, E Heijne, G Lindström, M Raymond, M Robbins, H Sadrozinski, P Sharp, K Smith, G Tonelli, T Tuuva, S Watts, P Weilhammer, R Wheadon. I am very grateful for the great help provided by P Brambilla. The literature is now extensive and I apologise to those whose contributions are inadequately represented. This review is based on accessible material and may not have given credit to work undertaken in the former Soviet Union; some recent references can be found in Edelman (1991).

Note added in proof. A related review, just received, which covers the use of the microstrip detectors described in this article for heavy quark physics studies at colliders is Schwarz (1994).

References

Adamovitch M *et al* 1990 *IEEE Trans. Nucl. Sci.* **37** 236–40
Adinolfi M *et al* 1993 *Nucl. Instrum. Methods* A **329** 117–24
Adolphsen C *et al* 1992 *Nucl. Instrum. Methods* A **313** 63–102
Adriani O *et al* 1993 *Nucl. Phys.* B (Proc. Suppl.) **32** 202–7
Agnew G *et al* 1993 *Proc. 26th Conf. on High Energy Physics (Dallas, TX)* ed J R Sandford (AIP Conf. Proc. **262**)
Alberganti R *et al* 1986 *Nucl. Instrum. Methods* A **248** 337–53
Albini E *et al* 1982 *Phys. Lett.* **110B** 339–43
Alfano B *et al* 1992 *Phys. Med. Biol.* **37** 1167–70
Allport P P *et al* 1991 *Nucl. Instrum. Methods* A **310** 155–9
—— 1993 *Nucl. Instrum. Methods* A **324** 34–52
Amendolia S R *et al* 1980a *Nucl. Instrum. Methods* **176** 449–56
—— 1980b *Nucl. Instrum. Methods* **176** 457–60
—— 1984 *Nucl. Instrum. Methods* **226** 117–21
—— 1990 *Nucl. Instrum. Methods* A **289** 539–42
Amidei D *et al* 1993 CDF/Pub/Sec VTX/Public 2168 *Nucl. Instrum. Methods* to be published
Angelini F *et al* 1989 *Nucl. Instrum. Methods* A **283** 755–61
—— 1993 *Nucl. Instrum. Methods* A **335** 69–77
Anghinolfi F *et al* 1992 *IEEE Trans. Nucl. Sci.* **39** 654–661

—— 1993a *RD-9 Status Report* CERN DRDC/93-17
—— 1993b *RD-19 Status Report* CERN DRDC/93-6
Anjos J *et al* 1987 *Phys. Rev. Lett.* **58** 311-4
Ansari R *et al* 1989 *Nucl. Instrum. Methods* A **279** 388-95
Anzivino G *et al* 1988 *Nucl. Instrum. Methods* A **263** 215-20
Appel J A 1992 *Ann. Rev. Nucl. Part. Sci.* **42** 637-99
Appelquist T, Barnett R M and Lane K 1978 *Ann. Rev. Nucl. Part. Sci.* **28** 387-499
Arens J F *et al* 1987 *Appl. Opt.* **26** 3846-51
Aspell P *et al* 1992 *Nucl. Instrum. Methods* A **315** 425-9
ATLAS 1992 *Letter of Intent* CERN/LHCC 92-4
Avset B S *et al* 1990 *IEEE Trans. Nucl. Sci.* **37** 1153-61
—— 1991 *Nucl. Instrum. Methods* A **310** 203-7
Bailey R *et al* 1983 *Nucl. Instrum. Methods* **213** 201-15
—— 1984 *Nucl. Instrum. Methods* **226** 56-8
—— 1984 *Phys. Lett.* **139B** 320-6
Barber G J *et al* 1987 *Nucl. Instrum. Methods* A **253** 530-6
Barkal O *et al 1990 SLAC-PUB-5358* Fort Worth Symposium pp 142-4
Bateman J E 1969 *Nucl. Instrum. Methods* **17** 256-60
Batignani G *et al* 1988 *Nucl. Instrum. Methods* A **273** 677-81
—— 1991 *Nucl. Instrum. Methods* A **310** 160-4
—— 1993 *Nucl. Instrum. Methods* A **326** 183-8
Beaumont S P *et al* 1992 *Nucl. Instrum. Methods* A **321** 172-9
—— 1993 *Nucl. Instrum. Methods* A **326** 313-8
Bebek C 1987 *Cornell University Report CLNS-87/67*
Beker H *et al* 1993 *Nucl. Instrum. Methods* A **332** 188-201
Belau E *et al* 1983 *Nucl. Instrum. Methods* A **214** 253-60
Bellini G, Foà L and Giorgi M 1982a *Phys. Rep.* **83** 9-38
Bellini G *et al* 1982b *Nucl. Instrum. Methods* **196** 351-60
—— 1984 *Nucl. Instrum. Methods* **225** 619-26
Benso S *et al* 1982 *Nucl. Instrum. Methods* **201** 329-33
Benvicelli W *et al* 1991 *Nucl. Instrum. Methods* A **310** 210-4
Berberis P *et al* 1993 *Nucl. Phys.* B (Proc. Suppl.) **32** 540-5
Beuville E *et al* 1990 *Nucl. Instrum. Methods* A **288** 157-67
Bichsel H 1988 *Rev. Mod. Phys.* **60** 663-99
Bingefors N *et al* 1993a *Nucl. Instrum. Methods* A **328** 447-71
—— 1993b *Nucl. Instrum. Methods* A **326** 112-9
Bocciolini M *et al* 1993 *Nucl. Phys.* B (Proc. Suppl.) **32** 77-82
Bosisio L 1993 *Proc. First Eur. Conf. on Large Scale Applications and Radiation Hardness of Semiconductor Detectors* (*Florence*) *Riv. Nuovo Cimento* to be published
Bouvier S *et al* 1993 *Nucl. Instrum. Methods* to be published
Bräuninger L *et al* 1993 *Nucl. Instrum. Methods* A **326** 129-35
Brenner R *et al* 1992 *Nucl. Instrum. Methods* A **315** 502-6
—— 1993a *Nucl. Instrum. Methods* A **326** 198-203
—— 1993b *CERN PPE/93-138 Nucl. Instrum. Methods* to be published
Bruzzi M *et al* 1993 *Nucl. Instrum. Methods* A **326** 344-9
Burger P 1984 *Nucl. Instrum. Methods* **226** 112-6
Buttler W *et al* 1988 *Nucl. Instrum. Methods* A **273** 778-83
Caccia M *et al* 1987 *Nucl. Instrum. Methods* A **260** 124-31
Carithers W *et al* 1989 *Nucl. Instrum. Methods* A **275** 89-96
Cesma G *et al* 1993 *Nucl. Phys.* B (Proc. Suppl.) **32** 546-54
Charpak G 1970 *Ann. Rev. Nucl. Sci.* **20** 195-254
Chen W *et al* 1993 *IEEE Trans. Nucl. Sci.* **39** 619-28
Chmill V B *et al* 1993 *Nucl. Instrum. Methods* A **326** 310-2
Chu S L *et al* 1972 *J. Appl. Phys.* **43** 3510-5
CMS 1992 *CMS Letter of Intent CERN/LHCC 92-3*
Culhane J L 1991 *Nucl. Instrum. Methods* A **310** 1-13
Cuzin M 1987 *Nucl. Instrum. Methods* A **253** 407-17
Dabrowski W and Korbel K 1989 *Nucl. Instrum. Methods* A **276** 270-9
Damerell C J S 1986 *Rutherford Appleton Laboratory Report RAL 86-077*

Damerell C J S *et al* 1987 *Nucl. Instrum. Methods* A **253** 478–81
—— 1989 *Nucl. Instrum. Methods* A **275** 484–93
—— 1990 *Nucl. Instrum. Methods* A **288** 236–9
Darbo G and Rossi L 1990 *Nucl. Instrum. Methods* A **289** 584–91
Dearnaley G and Northrop D C 1964 *Semiconductor Counters for Nuclear Radiations* (London: Spon)
Dentan M *et al* 1993 *Nucl. Phys.* B (Proc. Suppl.) **32** 530–4
Dierickx B *et al* 1993 *IEEE Trans. Nucl. Sci.* **39** 753–8
Dietl H *et al* 1987 *Nucl. Instrum. Methods* A **253** 460–6
Dorfan D 1993 *Nucl. Instrum. Methods* to be published
Drewery J S *et al Nucl. Instrum Methods* A **310** 165–70
Edelman V S (ed) 1991 *Instruments and Experimental Techniques* **34** 32–33
Edwards M, Hall G and Sotthibandhu S 1991 *Nucl. Instrum. Methods* A **310** 283–6
Ellett J *et al* 1992 *Nucl. Instrum. Methods* A **317** 28–46
Engels E *et al* 1987 *Nucl. Instrum. Methods* A **253** 523–9
England J B A *et al* 1981 *Nucl. Instrum. Methods* **185** 43–7
Equer B and Karar A 1988 *Nucl. Instrum. Methods* A **271** 574–84
—— 1989 *Nucl. Instrum. Methods* A **275** 558–63
Ewan G T 1979 *Nucl. Instrum. Methods* **162** 75–92
Faruqi A R 1991 *Nucl. Instrum. Methods* A **310** 14–23
Fernandez E *et al* 1990 *Nucl. Instrum. Methods* A **297** 153–62
Ferroni F *et al* 1991 *Nucl. Phys.* B (Proc. Suppl.) **23** 100–6
Fontaine A *et al* 1987 *Nucl. Instrum. Methods* A **253** 519–22
Franklin M *et al* 1992 *Nucl. Instrum. Methods* A **315** 39–42
Fretwurst E *et al* 1993 *Nucl. Instrum. Methods* A **326** 357–64
Gadomski S *et al* 1992 *Nucl. Instrum. Methods* A **320** 217–27
Galeema S 1985 *IEEE Trans Nucl. Sci.* **32** 417–8
Gatti E and Manfredi P F 1986 *Riv. Nuovo Cimento* **9** 1–146
Gatti E and Rehak P 1984 *Nucl. Instrum. Methods* **225** 608–14
Gatti E, Rehak P and Walton J 1984 *Nucl. Instrum. Methods* **226** 129–41
GEM 1992 *The GEM experiment at the SSC* Cal Tech. Report CALT-68-1826
Gill K *et al* 1992 *Nucl. Instrum. Methods* A **322** 177–88
Giubellino P *et al* 1989 *Nucl. Instrum. Methods* A **275** 89–96
Goldman L S and Totta P A 1983 *Solid State Tech* (June) 91–7
Gover J E and Srour J R 1985 *Basic radiation effects in nuclear power electronics technology* Sandia Labs Report SAND 85-0776
Goyot M and Jarron P 1984 *Nucl. Instrum. Methods* **226** 156–62
Halbert M L and Blankenship J L *Nucl. Instrum. Methods* **8** 106–16
Hall G 1984 *Nucl. Instrum. Methods* **220** 356–62
—— 1992 *Proc. Eur. Workshop on X-ray detectors for Synchrotron Radiation Sources (Aussois)* ed A H Walenta pp 129–39
Hall G, Vitè D and Wheadon R 1993 *Nucl. Instrum. Methods* A **326** 228–33
Hallewell G 1993 Proc. 3rd London Position Sensitive Detector Conf. *Nucl. Instrum. Methods* to be published
Hansen T-E 1985 *Nucl. Instrum. Methods* A **235** 249–53
Harrison R M 1988 *Phys. Med. Biol.* **33** 751–84
Heijne E H M 1983 *CERN Report 83-06*
Heijne E H M *et al* 1980 *Nucl. Instrum. Methods* **178** 331–43
Hikasa K *et al* 1992 Review of Particle Properties *Phys. Rev.* D **45** part II
Holl P *et al* 1989 *IEEE Trans. Nucl. Sci.* **NS-36** 251–5
Holland A D 1993 *Nucl. Instrum. Methods* A **326** 335–43
Holland S 1989 *Nucl. Instrum. Methods* A **275** 537–41
Holland S and Spieler H 1990 *IEEE Trans. Nucl. Sci.* **37** 463–8
Holmes-Siedle A and Adams L 1993a *Handbook of Radiation Effects* (Oxford: Oxford University Press)
Holmes-Siedle A *et al* 1993b *CERN-PPE/93-137 Nucl. Instrum. Methods* to be published
Horisberger R and Pitzl D 1993 *Nucl. Instrum. Methods* A **326** 92–9
Huhtinen M and Aarnio P 1993 *University of Helsinki report HU-SEFT R 1993-02. Nucl. Instrum. Methods* to be published
Huhtinen M *et al* 1993 *IEEE Trans. Nucl. Sci.* **40** 335–8
Kandiah K 1979 *Nucl. Instrum. Methods* **162** 699–718
Kaplan S N *et al* 1988 *Nucl. Instrum. Methods* A **273** 611–4

Kemmer J 1980 *Nucl. Instrum. Methods* **169** 499–502
—— 1984 *Nucl. Instrum. Methods* **226** 89–93
Kemmer J and Lutz G 1987 *Nucl. Instrum. Methods* A **253** 365–77
Kemmer J *et al* 1990 *Nucl. Instrum. Methods* A **288** 92–8
Kenney C *et al* 1993 *Nucl. Phys.* B (Proc. Suppl.) **32** 460–7
Klanner R 1988 *Instrumentation in Elementary Particle Physics* ed C Fabjan and J Pilcher (Singapore: World Scientific) pp 150–73
Kleinfelder S *et al* 1988 *IEEE Trans. Nucl. Sci.* **35** 171–5
Konozenko I, Semenyuk A and Khivrich V 1971 *Radiation Effects in Semiconductors* ed J Corbett and G Watkins (New York: Gordon and Breach) pp 249–55
Laakso M *et al* 1993 *Nucl. Instrum. Methods* A **327** 517–22
Laegsgard E 1979 *Nucl. Instrum. Methods* **162** 93–112
Landau 1944 *J. Phys. (USSR)* **8** 201–5
Landolt-Börnstein 1985 *Numerical Data and Functional Relationships in Science and Technology* vol 17 (Berlin: Springer)
Lechner P *et al* 1993 *Nucl. Instrum. Methods* A **326** 284–9
Lohstroh J *et al* 1981 *Solid State Electron.* **24** 805–14
Luke P N *et al* 1985 *IEEE Trans. Nucl. Sci.* **32** 457–62
Ma T P and Dressendorfer P (ed) 1988 *Ionising Radiation Effects in MOS Devices and Circuits* (New York: Wiley)
Manfredi P F 1983 *Miniaturisation of High Energy Physics Detectors* ed A Stefanini (New York: Plenum) pp 77–86
Marciano W J 1991 *Ann. Rev. Nucl. Part. Sci.* **41** 469–509
Mayer J W 1959 *J. Appl. Phys.* **30** 1937–44
McGregor D S *et al* 1992 *Nucl. Instrum. Methods* A **322** 487–92
McKay K G 1951 *Phys. Rev.* **84** 829–32
McKenzie J M 1979 *Nucl. Instrum. Methods* **162** 49–74
Messenger G C and Ash M S 1986 *The Effects of Radiation on Electronic Systems* (New York: Van Nostrand Reinhold)
Möschen J *et al* 1990 *Nucl. Instrum. Methods* A **288** 180–6
Moser H-G *et al* 1991 *Nucl. Instrum. Methods* A **310** 490–2
Munday D *et al* 1993 *Nucl. Instrum. Methods* A **326** 100–11
Nicholson P W 1974 *Nuclear Electronics* (New York: Wiley)
Nygård E *et al* 1991 *Nucl. Instrum. Methods* A **301** 506–16
Oed A 1988 *Nucl. Instrum. Methods* A **263** 351–9
Olsen A *et al* 1989 *Proc. ECFA Study Week (Barcelona)* CERN 89–10 pp 678–9
Parker S 1989 *Nucl. Instrum. Methods* A **275** 494–516
Pedder D J 1988 *Hybrid Circuits* **15** 4–7
Peisert A 1992 *Instrumentation in High Energy Physics* ed F Sauli (Singapore: World Scientific)
Perez-Mendez V *et al* 1986 *Nucl. Instrum. Methods* A **252** 478–82
Pinotti E *et al* 1993 *Nucl. Instrum. Methods* A **326** 85–91
Pitzl D *et al* 1991 *Nucl. Phys.* B (Proc. Suppl.) **23A** 340–6
—— 1992 *Nucl. Instrum. Methods* A **311** 98–104
Popovic R S 1991 *Hall Effect Devices* (Bristol: Adam Hilger)
Radeka V 1968 *IEEE Trans. Nucl. Sci.* **NS-15** 455–70
—— 1974 *IEEE Trans. Nucl. Sci.* **NS-21** 51–64
—— 1988 *Ann. Rev. Nucl. Sci. Part.* **38** 217–77
Radeka V *et al* 1988 *IEEE Trans. Nucl. Sci.* **35** 155–9
—— 1993 *Nucl. Instrum. Methods* A **326** 77–81
Ravi K 1981 *Imperfections and Impurities in Semiconductor Silicon* (New York: Wiley)
Raymon D M *et al* 1991 *Nucl. Instrum. Methods.* A **310** 552–8
Rehak P *et al* 1985 *Nucl. Instrum. Methods* A **235** 224–34
—— 1986 *Nucl. Instrum. Methods* A **248** 367–78
—— 1989 *IEEE Trans. Nucl. Sci.* **36** 203–9
Roy T, Watts S J and Wright D 1989 *Nucl. Instrum. Methods.* A **275** 545–57
Sadrozinski H *et al* 1993 *Nucl. Instrum. Methods* to be published
Schwarz A 1992 *Max Planck Institute Report MPI-PhE/92-05*
—— 1994 *Max Planck Institute Report MPI-PhE/93-28. Phys. Rep.* to be published
SDC 1992 *SDC Technical Design Report SDC-92-201, SSC Lab Report SSCL-SR-1215*

Selberherr S 1984 *Analysis and Simulation of Semiconductor Devices* (Wien: Springer)
Shapiro S *et al* 1990 *Fort Worth Symposium* SLAC-PUB-5357 pp 142–4
Shapiro S L *et al* 1989 *Nucl. Instrum. Methods* A **275** 580–6
—— 1990 *Fort Worth Symposium* SLAB-PUB-5357 p 1990
Shockley W 1950 *Electrons and Holes in Semiconductors* (New York: Van Nostrand)
Sidwell R A, Reay N W and Stanton N 1983 *Ann. Rev. Nucl. Part. Sci.* **33** 539–68
Sigfridson B and Lindström J 1976 *J. Appl. Phys.* **47** 4611–20
Singh M and Doria D 1983 *Med. Phys.* **10** 421–35
Snoeys W *et al* 1992 *IEEE Trans Nucl. Sci.* **39** 1263–9
—— 1993 *Nucl. Instrum. Methods.* A **326** 144–9
Solomon C J and Ott R J 1988 *Nucl. Instrum. Methods* A **273** 787–92
Spieler H 1991 *Subsystem R&D Progress Report for a Silicon Tracking System* University of California Santa Cruz Report SCIPP 91/28
Spooner N J C *et al* 1991 *Nucl. Instrum. Methods* A **310** 227–31
Stanton J C 1989 *IEEE Trans. Nucl. Sci.* **36** 522–5
Stefanini G *et al* 1993 *Nucl. Instrum. Methods* to be published
Street R A 1983 *Phys. Rev.* B **27** 4924–32
Strüder L *et al* 1987 *Nucl. Instrum. Methods* A **253** 386–92
—— 1988 *IEEE Trans. Nucl. Sci.* **35** 372–6
—— 1989 *Nucl. Instrum. Methods* A **283** 387–98
—— 1990 *Nucl. Instrum. Methods* A **288** 227–35
Sumner T *et al 1993 Proc. 3rd London Position Sensitive Detector Conf. Nucl. Instrum. Methods* to be published
Sze S M (ed) 1988 *VLSI Technology* (New York: McGraw Hill)
Sze S M 1981 *Physics of Semiconductor Devices* (New York: Wiley)
Tedja S *et al* 1992 *Nucl. Instrum. Methods* A **312** 576–84
Turchetta R 1993 *Nucl. Instrum. Methods* A **335** 44–58
Vacchi A *et al* 1993 *Nucl. Instrum. Methods* A **326** 267–72
Van Ginneken A 1989 *Fermilab Note* FN-522
Van Lint V A J 1987 *Nucl. Instrum. Methods* A **253** 453–9
von Ammon W and Herzer H 1984 *Nucl. Instrum. Methods* **226** 94–102
Walker J T *et al* 1984 *Nucl. Instrum. Methods* **226** 200–3
Warburton K *et al* 1993 *Proc. 3rd London Position Sensitive Detector Conf. Nucl. Instrum. Methods* to be published
Wells A 1993 *Proc. 3rd London Position Sensitive Detector Conf. Nucl. Instrum. Methods* to be published
Wells A and Pounds K 1993 *Phys. World* **6** 32–5
Wright W, Millaud J and Nygren D 1993 *Nucl. Phys.* B (Proc. Suppl.) **32** 468–79
Wunstorf R *et al* 1990 *Proc. of Aachen LHC Workshop* CERN 90-10, vol 3, pp 706–20
Yamamoto K *et al* 1993 *Nucl. Instrum. Methods* A **326** 222–7
Ziock H J *et al* 1990 *IEEE Trans. Nucl. Sci.* **37** 1238–42
—— 1993 *IEEE Trans. Nucl. Sci.* **40** 344–8